UNIVERSITY OF AMSTERDAM

UvA-DARE (Digital Academic Repository)

Employing nanomedicine in inflammatory diseases

van Leent, M.M.T.

Publication date
2021

Link to publication

Citation for published version (APA):
van Leent, M. M. T. (2021). *Employing nanomedicine in inflammatory diseases*.

9 | Prosaposin Mediates Inflammation in Atherosclerosis

Mandy M.T. van Leent, Thijs J. Beldman, Yohana C. Toner, Marnix A. Lameijer, Nils Rother, Siroon Bekkering, Abraham J.P. Teunissen, Xianxiao Zhou, Roy van der Meel, Joost Malkus, Sheqouia A. Nauta, Emma D. Klein, Francois Fay, Brenda L. Sanchez-Gaytan, Carlos Pérez-Medina, Ewelina Kluza, Yu-Xiang Ye, Gregory Wojtkiewicz, Edward A. Fisher, Filip K. Swirski, Matthias Nahrendorf, Bin Zhang, Yang Li, Bowen Zhang, Leo A.B. Joosten, Gerard Pasterkamp, Arjan Boltjes, Zahi A. Fayad, Esther Lutgens, Mihai G. Netea, Niels P. Riksen, Willem J.M. Mulder, Raphaël Duivenvoorden

ABSTRACT

Macrophages play a central role in the pathogenesis of atherosclerosis. The inflammatory properties of these cells are dictated by their metabolism, of which the mechanistic target of rapamycin (mTOR) signaling pathway is a key regulator. Using myeloid cell-specific nanobiologics in apolipoprotein E-deficient ($Apoe^{-/-}$) mice, we found that targeting the mTOR and ribosomal protein S6 kinase-1 (S6K1) signaling pathways rapidly diminishes plaque macrophages' inflammatory activity. By investigating transcriptome modifications, we identified *Psap*, a gene encoding for prosaposin, to be closely related with mTOR signaling. Subsequent *in vitro* experiments revealed that *Psap* inhibition suppresses both glycolysis and oxidative phosphorylation. Transplantation of $Psap^{-/-}$ bone marrow to LDL receptor knock-out ($Ldlr^{-/-}$) mice led to a reduction of atherosclerosis development and plaque inflammation. Finally, we confirmed the relationship between *PSAP* expression and inflammation in human carotid atherosclerotic plaques. Our findings provide mechanistic insights into the development of atherosclerosis, and identify prosaposin as a potential therapeutic target.

INTRODUCTION

Atherosclerosis is a lipid-induced chronic inflammatory condition and the underlying cause of myocardial infarction and stroke. It is caused by the focal accumulation of lipoproteins in the arterial subendothelial space. After oxidative modification, lipoproteins act as danger associated molecular patterns (DAMPs) triggering an inflammatory response with macrophages as the main protagonists [1].

The activation of macrophages by oxidized low-density lipoprotein (oxLDL) and cholesterol crystals is an energy-demanding process and requires adjustment of their metabolism [2–4]. In fact, recent studies revealed that metabolic reprogramming dictates the phenotype and inflammatory response of macrophage subsets in plaques, and that the metabolic signature of macrophages is associated with the vulnerability of plaques for rupture [3–5]. Unraveling the regulation of plaque macrophage metabolism is therefore of fundamental importance and may uncover new targets for therapy.

In the present study we investigated the mechanistic target of rapamycin (mTOR) signaling pathway in plaque macrophages. mTOR is at the heart of orchestrating cell metabolism and inflammatory activity in macrophages [6]. However, mTOR's role in regulating immunometabolism in atherosclerosis is poorly understood [6]. Here, we investigated the role of mTOR signaling in atherosclerosis-prone apolipoprotein E-deficient (*Apoe*^{-/-}) mice, through inhibition of mTOR or its downstream target ribosomal protein S6 kinase-1 (S6K1). To achieve specific inhibition, we intravenously administered two different myeloid cell-specific nanobiologics that respectively target mTOR or S6K1. We observed a consistent reduction of plaque inflammation across multiple modalities and readouts. Subsequently, we unraveled the molecular mechanisms underlying this anti-inflammatory effect by transcriptome analyses of myeloid cells isolated from plaques. *Psap* surfaced as a key-regulating gene. This gene encodes prosaposin, a highly conserved lysosomal protein involved in glycosphingolipid metabolism. As its role in atherosclerosis is unknown, we set out to study how prosaposin mediates inflammation in monocytes and macrophages. We performed *in vitro* metabolic analyses and studies on plaque development using *Psap* knockout mice. In addition, we investigated the role of *PSAP* in human atherosclerosis by functional assays, histology and single-cell transcriptome analysis of plaques.

9

RESULTS

mTORi- and S6K1i-targeted nanobiologic therapies reduce plaque inflammation

In addition to monocytes and macrophages, other cell types, including T cells, endothelial cells and smooth muscle cells, play pivotal roles in the pathogenesis of atherosclerosis [1]. As mTOR signaling is essential to cell metabolism [7], systemic mTOR inhibition will affect all cell types involved in atherogenesis. We aimed to investigate the effect of inhibiting the mTOR pathway specifically in monocytes and macrophages. To achieve this, we developed an apolipoprotein A1-based nanobiologic that facilitates drug delivery to myeloid cells with high targeting efficiency [8,9]. We formulated nanobiologics containing the mTOR inhibitor rapamycin (mTORi-NB), and the S6K1 inhibitor PF-4708671 (S6K1i-NB) [10] (**Figure S1A**). *Ex vivo* near-infrared fluorescence (NIRF) imaging performed 24 hours after intravenous administration showed that DiR-labeled nanobiologics primarily accumulate in the liver, spleen and kidneys of *Apoe*^{-/-} mice (**Figures S1B** and **S1C**). High DiR uptake was observed in the aortic sinus area (**Figure S1D**), which is the preferential site of plaque development in this mouse model. Immune cell specificity was evaluated by flow cytometry using mTORi-NB and S6K1i-NB labeled with the fluorophore DiO. Similar to previous studies [8,9], both nanobiologics were predominantly taken up by aortic macrophages, Ly6C^{hi} monocytes, neutrophils, and dendritic cells (**Figures S1E** and **S1F**). Non-myeloid cells (Lin[+]) took up a negligible amount of the nanobiologics. In blood, spleen and bone marrow, we identified a similar myeloid cell-biased uptake pattern (**Figure S1G**).

We studied the effect of mTORi- and S6K1i-NB treatment on plaque inflammation in 20-week old *Apoe*^{-/-} mice that had been fed a Western diet (WD) for 12 weeks to develop atherosclerotic lesions. While they remained on a WD, all mice were treated with four intravenous injections of phosphate-buffered saline (PBS used as control), unloaded nanobiologics, mTORi-NB (containing 5 mg/kg rapamycin), or S6K1i-NB (containing 5 mg/kg PF-4708671) over the course of one week (**Figure 1A**). We verified that mTORi-NB treatment did not affect serum cholesterol levels (**Figure S1H**). Mice treated with mTORi-NB had a 14% (P<0.0001) and 9% (P=0.006) smaller plaque size as compared to animals treated with PBS and unloaded NB, respectively (**Figures 1B-D**). Plaque collagen content was not affected by mTORi-NB, while macrophage content was reduced by 33% (P=0.013) and 34% (P=0.004) as compared to both control groups (**Figures 1E, 1F, S2A**). S6K1i-NB treatment showed a similar effect on plaque inflammation with a 20% (P=0.046) reduction in plaque macrophage content as compared to PBS-treated mice (**Figures 1E** and **1F**), while no effect on

plaque size and collagen content was observed (**Figures 1B**, **1D** and **S2A**). These data indicate that mTORi-NB and S6K1i-NB treatment ameliorated plaque vulnerability by reducing macrophage rich areas without affecting collagen content (**Figure S2B**).
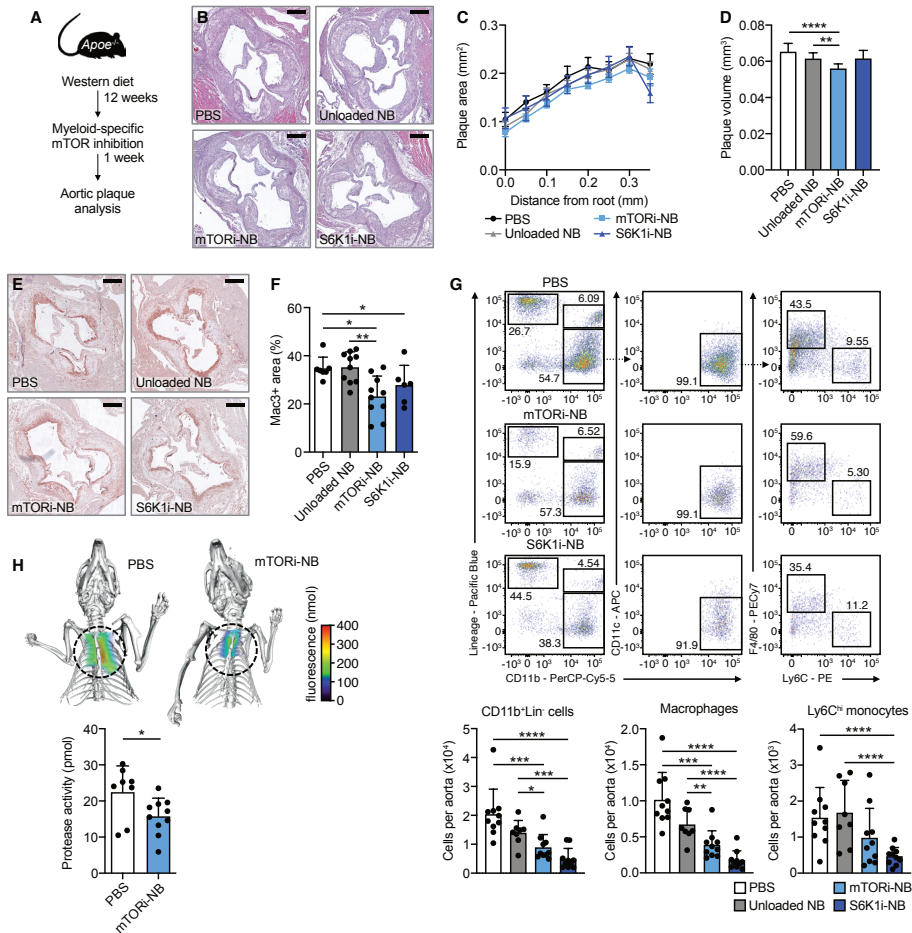
Figure 1. Myeloid specific mTOR inhibition reduces atherosclerotic plaque inflammation. *Apoe^{-/-}* mice were kept on a Western diet for 12 weeks, followed by 1 week of treatment, while continuing the diet. Treatment consisted of 4 intravenous injections of control (PBS), unloaded nanobiologics, mTORi-NB or S6K1i-NB. See schematic in (**A**). (**B**) Representative images of H&E stained aortic roots. (**C**) Histologic quantification of plaque area at set distances from the aortic root, presented as mean ± SEM (n=6-10 per group). (**D**) Lesion volume was calculated as area under the curve in **C**. (**E**) Representative Mac3 stained aortic roots and (**F**) quantification of Mac3 positive area of mTORi-NB and S6K1i-NB treated mice (n=6-10 per group). (**G**) Representative flow cytometry plots and quantification of CD11b+Lin- cells, macrophages (CD11b+Lin-CD11c-F4/80+Ly6C^{lo}) and Ly6C^{hi} monocytes (CD11b+Lin-CD11c-F4/80-Ly6C^{hi}) in the aorta (n=8-10 per group). (**H**) FMT/CT imaging showed decreased protease activity in the aortic root in mTORi-NB treated mice (n=8-10 per group). Data are presented as mean ± SD unless otherwise stated. *p<0.05, **p<0.01, ***p<0.001, ****p<0.0001.

The histology results were corroborated by flow cytometry of whole aortas. After one week of treatment, mTORi-NB reduced the number of aortic CD11b$^+$Lin$^-$ cells (monocytes and macrophages) by 56% (P=0.0005) and 36% (P=0.027), as compared to control (PBS) and unloaded nanobiologics, respectively (**Figures 1G** and **S2C**). This effect was mainly driven by a reduction in plaque macrophages. Aortic CD11b$^+$Lin$^-$ cells were also markedly decreased in the S6K1i-NB treated mice, by 76% (P<0.0001) and 65% (P=0.0005) in comparison to the control and unloaded nanobiologic-treated groups (**Figures 1G** and **S2C**). In this treatment group both macrophage and Ly-6C^{hi} monocyte numbers were reduced. Analysis of myeloid cell populations in the bone marrow, spleen and peripheral blood indicated that the inhibition of plaque inflammation could not be explained by suppressed myelopoiesis, as neutrophils, Ly6C^{lo} and Ly6C^{hi} monocytes were equal or increased in the nanobiologic-treated mice (**Figures S3A-C**).

To test the plaque's inflammatory activity, we performed *in vivo* fluorescence molecular tomography with computed tomography (FMT-CT) imaging to quantify protease activity in the aortic sinus area. We used the same mouse model and treatment regimen as described above (**Figure 1A**). Control and mTORi-NB treated *Apoe$^{-/-}$* mice received a single injection of an activatable pan-cathepsin protease sensor 24 hours before imaging. The protease sensor is taken up by activated macrophages and cleaved in the endolysosome [11], yielding fluorescence as a function of enzyme activity. mTORi-NB reduced protease activity by 30% compared to control (P=0.03, **Figure 1H**).

Taken together, these data show that myeloid-specific inhibition of the mTOR signaling pathway rapidly reduces inflammatory activity in atherosclerotic lesions. This incentivized us to unravel the underlying molecular mechanisms.

mTOR and S6K1 inhibition downregulate Psap in plaque macrophages

To gain insight into the mechanism by which mTOR-S6K1 signaling affects monocytes and macrophages in atherosclerosis, we used laser capture microdissection (LCM) to isolate CD68 positive cells from aortic sinus plaques of *Apoe$^{-/-}$* mice that were treated for one week with either PBS (control), mTORi-NB or S6K1i-NB. Total RNA of these cells was isolated for sequencing and whole transcriptome analysis.

First, we assessed if the reduced plaque monocyte and macrophage burden could be explained by diminished monocyte recruitment or was potentially mediated by autophagy, since the latter can be induced by mTOR inhibition [12]. Both mechanisms

did not provide a satisfactory explanation. We found no inhibiting effect of our nanobiologic treatments on chemokine related gene expression (**Tables S1** and **S2**). mTORi-NB treatment did not affect autophagy related gene expression (**Table S3**). In the S6K1i-NB treated group, five genes were differentially expressed, of which two were up-regulated and three were down-regulated (**Table S4**). The current data do not allow for definitive conclusions regarding the effects of our nanobiologics on autophagy. Autophagy plays a crucial role in atherosclerosis, and potential effects of our nanobiologics on this process require further investigation in future studies. Subsequently, we adopted a systems biology approach of weighted gene co-expression network analysis (WGCNA) in which a co-expression network is constructed based on expression correlation between genes. We used topological overlap matrix (TOM) plots to show correlations among all genes, in which increased color intensity indicates strong correlation coefficients between genes. To identify modules with groups of strongly co-expressed genes, we used linkage hierarchical clustering to group genes based on their topological overlap with other genes. We then ranked the modules by the significance of enrichment with the differentially expressed genes (DEGs) between treatments and controls. For both the mTORi-NB- and S6K1i-NB-treated mice, the '*turquoise*' modules were of highest interest, as DEGs were most significantly enriched in these modules. The mTORi-NB *turquoise* module contained 1052 genes, which significantly enriched with 46% of the DEGs (fold enrichment = 5.90, adjusted P = $9.75×10^{-20}$, **Figure 2A** and **2B**). The S6K1i-NB *turquoise* module consisted of 1825 genes, which significantly enriched with 51% of the DEGs (fold enrichment = 3.76, adjusted P = $1.80×10^{-154}$, **Figure 2C** and **2D**). Gene ontology analysis of both *turquoise* modules showed most pronounced enrichment of genes in cellular processes (GO:0009987) and metabolic processes (GO:0008152).

Next, we identified intramodular hub genes in both the mTORi-NB and S6K1i-NB *turquoise* modules. For this purpose, we selected the top 10% genes of the *turquoise* module with the highest connectivity index. Of these highly connected genes the ones with highest significance and fold change in expression were considered likely to be key regulators in the modules and can provide important biological insights (**Figure 2E** and **2F**) [13]. We identified four down-regulated hub genes (*Psap, Cox7c, Rsrp1* and *Ctsb*) and three up-regulated hub genes (*Flna, Synpo* and *Hspg2*) (**Figure 2E, Table S5**) in the mTORi-NB *turquoise* module. In the S6K1i-NB *turquoise* module we identified five down-regulated hub genes (*Psap*, Cox7c, *Hnmpf, Rps27a, Lyz1*) and two up-regulated hub genes (*Arhgdia, Rn45s*) (**Figure 2F, Table S6**). Interestingly, *Psap* and *Cox7c* were consistently down-regulated by both mTOR and S6K1 inhibition. *Psap* encodes prosaposin, which is a proprotein for the saposins A to D, and is essential in lysosomal glycosphingolipid degradation [14]. *Cox7c* encodes the cytochrome c oxidase

subunit 7C which is a component of the mitochondrial respiratory chain. Next, we performed a Multiscale Embedded Gene Co-expression Network Analysis (MEGENA) of the *turquoise* modules, as an additional method to identify biologically meaningful hub genes. While *Cox7c* was not identified by this analysis, *Psap* was confirmed as an important hub gene that was downregulated in response to both mTOR and S6K1 inhibition (**Figures 2G** and **2H**), making *Psap* the prime candidate for further analysis. So far, its role in atherosclerosis is unknown.

The decrease in *Psap* transcription that we observed in the transcriptome analysis also translated into diminished protein expression of prosaposin. We performed histologic staining of prosaposin on cross-sections of the aortic sinus area of *Apoe*^{-/-} mice with advanced lesions. Indeed, we observed widespread prosaposin expression in plaques (**Figure 2I**), with a high degree of macrophage co-localization (**Figure S4**). Prosaposin expression in plaques of mice that were either treated with mTORi-NB or S6K1i-NB was reduced by 55% and 33%, respectively, as compared to control (**Figure 2J**).

## Silencing Psap expression affects immunometabolism

Stimulation of monocytes with oxLDL upregulates aerobic glycolysis as well as oxidative phosphorylation [15]. Since we found the effects of mTOR inhibition to be associated with *Psap*, we were prompted to investigate if *Psap* expression affects cellular metabolism. For this purpose, we formulated lipid nanoparticles containing small interfering RNA that targets *Psap* (*Psap* siRNA-LNPs), as previously described [16]. The effect of *Psap* siRNA-LNPs on metabolic reprogramming was assessed *in vitro* in bone marrow-derived macrophages by extracellular flux analysis. Changes in extracellular acidification rate (ECAR) in response to glucose and oligomycin (OM) injection were used to calculate glycolysis parameters. Changes in oxygen consumption rate (OCR) in response to OM, carbonyl cyanide 4-(trifluoromethoxy)phenylhydrazone (FCCP), and rotenone (ROT) + antimycin A (AA) injection were used to calculate oxidative phosphorylation parameters.

We found that silencing of *Psap* expression suppresses glycolysis (**Figure 3A**) as well as oxidative phosphorylation parameters (**Figure 3B**), when compared to control and control (Ctrl) siRNA-LNPs. These results mirror the effects of mTOR inhibition (rapamycin) and S6K1 inhibition (PF-4708671) on glycolysis (**Figure 3C**) and oxidative phosphorylation (**Figure 3D**). Together these data indicate that *Psap* expression affects cell metabolism, which may explain the mechanism by which *Psap* regulates inflammatory activity of monocytes and macrophages.
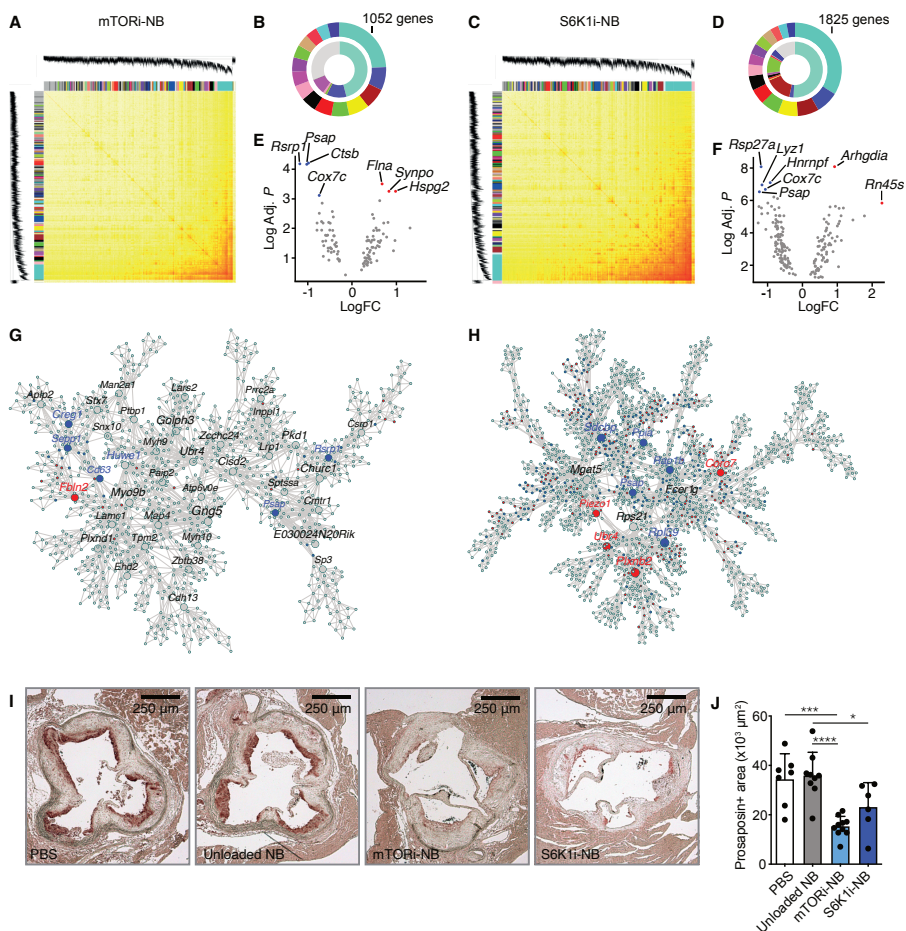
Figure 2. Effect of mTOR inhibition on plaque macrophage transcriptome. Transcriptome analysis was performed on CD68^{+} cells isolated from aortic roots of *Apoe^{-/-}* mice after mTORi-NB (**A,B,E,G**) or S6K1i-NB (**C,D,F,H**) treatment, as compared to control. (n=8-10 per group). (**A,C**) Topological overlap matrix. Each row and column of the heatmap represent a single gene, with the color intensity indicating the network connection strength. The dendrograms on the upper and left sides show the hierarchical clustering tree of genes. (**B,D**) The fifteen modules with the highest connectivity are ordered by size (outer ring). The inner ring shows differentially expressed genes within a module, as a percentage of total number of differentially expressed genes. (**E,F**) Volcano plot of genes within the *turquoise* module with the highest connectivity. Hub gene are identified based on p-value and fold change. The up- and downregulated hub genes are shown in red and blue, respectively. (**G,H**) MEGENA network of the *turquoise* module. Up- and downregulated genes are shown in red and blue, respectively. (**I,J**) *Apoe^{-/-}* mice were fed a Western diet for 12 weeks, followed by 1 week of treatment, while kept on a Western diet. Treatment consisted of 4 intravenous injections of control (PBS), unloaded nanobiologics, mTORi-NB or S6K1i-NB. Aortic roots were harvested for histological analysis. (**I**) Representative images of prosaposin staining of the aortic root and (**J**) quantification of prosaposin positive areas within the plaque (n=6-10 per group). Data are presented as mean ± SD. *p<0.05, **p<0.01, ***p<0.001, ****p<0.0001.
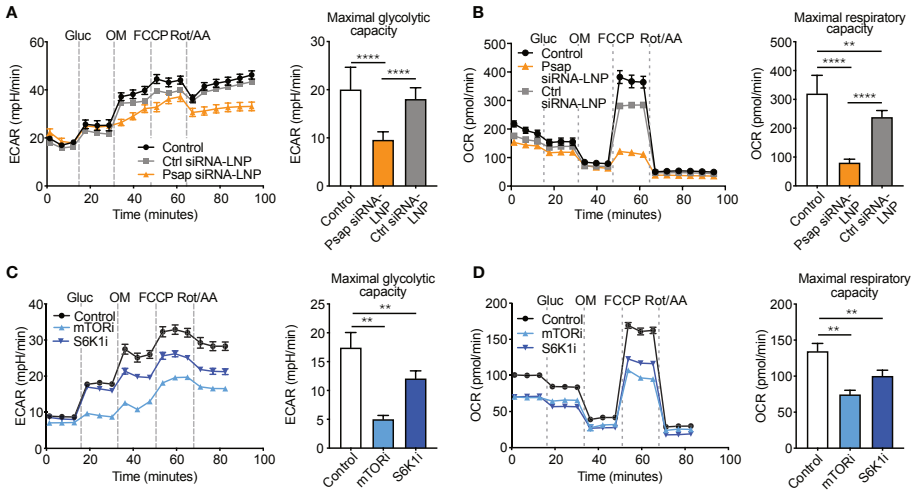
Figure 3. *Psap* **affects immunometabolism.** (**A-B**) Murine bone marrow-derived macrophages were incubated with *Psap* small interfering RNA lipid nanoparticles (*Psap* siRNA-LNPs) or control (Ctrl) siRNA-LNPs and subjected to a metabolic assay (n=10 per condition). *Psap* inhibition through *Psap* siRNA-LNPs decreases the maximal glycolytic capacity (**A**) and maximal respiratory capacity (**B**) of murine bone marrow-derived macrophages. (**C-D**) Murine bone marrow-derived macrophages were incubated with mTOR or S6K1 inhibitors (both 20 μM) and subjected to a metabolic assay (n=6 per condition). Both mTOR and S6K1 inhibition decrease the maximal glycolytic capacity (**C**) and maximal respiratory capacity (**D**). Line graphs are presented as mean ± SEM, bar graphs are presented as mean ± SD. *p<0.05, **p<0.01, ***p<0.001, ****p<0.0001.

Psap expression mediates inflammation in experimental atherosclerosis

To assess the role of *Psap* in atherosclerosis development and plaque inflammation, we transplanted bone marrow from *Psap*^{-/-} into lethally irradiated *Ldlr*^{-/-} mice. *Apoe*^{-/-} mice are unsuitable for this purpose, as transplantation of bone marrow producing Apolipoprotein E would affect serum lipid levels and prohibit the development of atherosclerosis [17]. Mice that received *Psap*^{+/+} bone marrow cells served as controls (**Figure 4A**). Mice were put on a Western diet for 11 weeks in order to develop atherosclerotic lesions. Serum cholesterol levels were equal in both groups (**Figure S5A**). We performed quantitative histologic analysis of plaques in the aortic sinus area by serial cross sectioning at set distances from the aortic root. Cross-sections were stained with Hematoxylin and Eosin (H&E, **Figure 4B**). Lesion volume was calculated from the area under the curve (**Figure 4C**). *Psap*^{-/-} transplanted mice showed a 22.8% (P<0.0001) reduction in plaque volume as compared to *Psap*^{+/+} transplanted animals (**Figure 4D**). There was no difference in the collagen content of the plaques, as assessed by Sirius red staining (**Figure 4E** and **4F**).
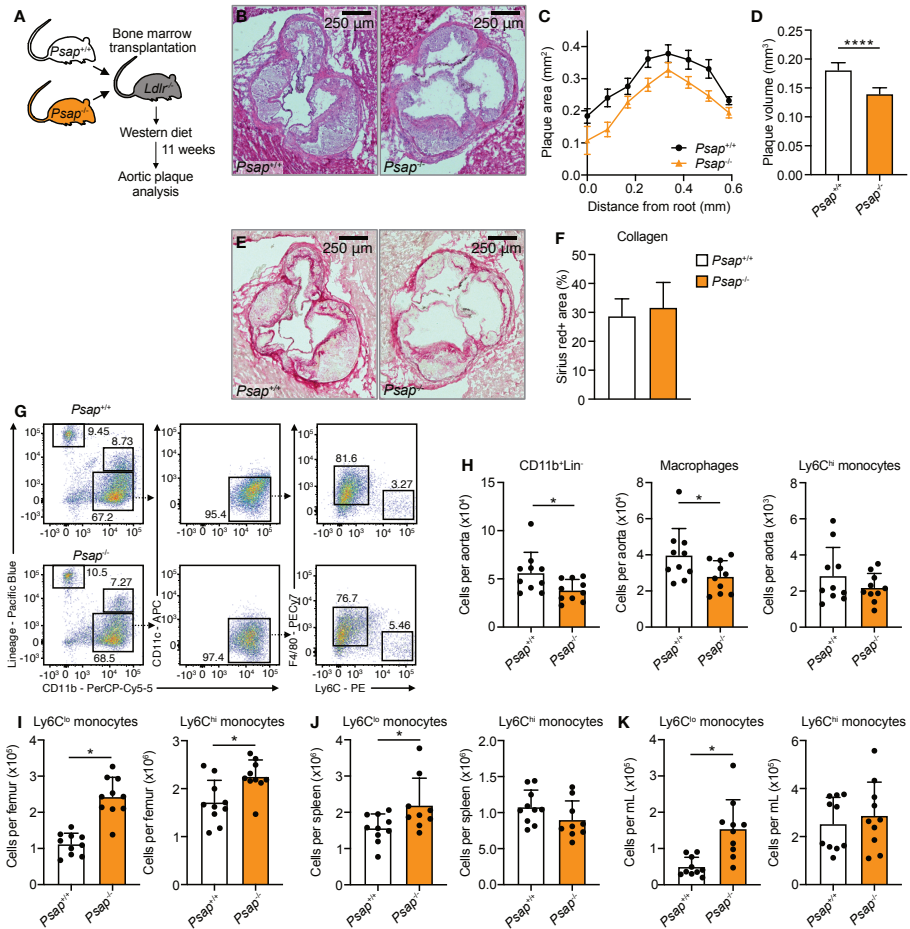
Figure 4. *Psap* **mediates atherosclerotic plaque inflammation in** *Ldlr*^{-/-} **mice.** *Ldlr*^{-/-} mice were lethally irradiated and transplanted with *Psap*^{+/+} or *Psap*^{-/-} bone marrow cells. Mice were left to reconstitute for 6 weeks after which they were put on a Western diet for 11 weeks (n=10 per group for all panels). (**A**) Schematic of experimental setup. (**B**) Representative images H&E stained aortic roots. (**C**) Histologic quantification of plaque area at set distances from the aortic root, presented as mean ± SEM. (**D**) Lesion volume was calculated as area under the curve in **C**, this shows that *Psap*^{-/-} transplanted mice developed smaller plaques. (**E**) Representative images of Sirius red-stained aortic roots. (**F**) Histologic quantification of plaque collagen content. (**G**) Representative flow cytometry plots and (**H**) quantification of CD11b^{+}Lin^{-} cells, macrophages (CD11b^{+}Lin^{-}CD11c^{-}F4/80^{+}Ly6C^{lo}) and Ly6C^{hi} monocytes (CD11b^{+}Lin^{-}CD11c^{-}F4/80^{-}Ly6C^{hi}) in the aorta. Quantification of Ly6C^{lo} and Ly6C^{hi} monocytes in the bone marrow (**I**), spleen (**J**) and blood (**K**). Data are presented as mean ± SD unless otherwise stated, *p<0.05, **p<0.01, ***p<0.001, ****p<0.0001.

Subsequently we focused on quantifying immune cells in atherosclerotic lesions by flow cytometry of whole aortas. Again, lethally irradiated *Ldlr*^{-/-} mice received either *Psap*^{-/-} or *Psap*^{+/+} bone marrow and were put on a Western diet for 11 weeks. Aortic plaques of *Psap*^{-/-} transplanted mice contained 32.4% (P=0.04) less CD11b^{+}Lin^{-} cells, primarily caused by a reduction in plaque macrophages, as well as 32.9% (P=0.02)

less neutrophils when compared to *Psap*^{+/+} transplanted animals (**Figures 4G, 4H and S5B**). The number of non-myeloid cells (Lin⁺ cells) was unaffected (**Figure S5B**). These data indicate a reduction of plaque inflammation in mice that received *Psap*^{-/-} bone marrow.

We investigated if these changes in plaque size and myeloid cell content were the result of systemic immune effects. There was no difference in numbers of Lin⁻Sca1⁺c-kit⁻ (LSK) cells or proliferation rates of multipotent progenitors (MPP) (**Figures S5C-E**). Interestingly, Ly6C^{hi} as well as Ly6C^{lo} monocyte counts were increased in the bone marrow (**Figure 4I**), while Ly6C^{lo} monocytes were increased and Ly6C^{hi} monocytes unchanged in the blood and spleen (**Figures 4J and 4K**). Together, these results show that myelopoiesis in Psap^{-/-} transplanted mice was not suppressed. The increase in Ly6C^{lo} monocyte counts in the bone marrow, blood and spleen of Psap^{-/-} transplanted mice (**Figures 4I-K**) may contribute to a beneficial effect on plaque inflammation since these cells play a critical role in tissue homeostasis and repair [18]. Concerning the neutrophils, we did not observe changes in the circulation, the spleen and bone marrow which could explain the lower neutrophil number in the plaques (**Figure S5F**).

Together, our data show that plaque inflammation and atherosclerosis development is reduced in *Ldlr*^{-/-} mice receiving *Psap*^{-/-} bone marrow. This underscores the finding of our transcriptome analysis that in myeloid cells, *Psap* plays a key role in atherosclerosis.

Prosaposin and inflammation in human atherosclerosis

Prosaposin is highly conserved during evolution and is found in all bony vertebrates [19]. Since the function of prosaposin is similar in mice and man, we were interested in the involvement of prosaposin in human atherosclerosis.

First, we investigated the role of prosaposin in oxLDL priming of human myeloid cells. We stimulated primary human monocytes *in vitro* with oxLDL or RPMI (control) for 24 hours. Cells rested for 5 days after which they were re-stimulated with LPS or Pam3Cys (**Figure S6A**). OxLDL primed cells displayed a higher cytokine response as compared to control cells (**Figure 5A** and **S6B**). When oxLDL stimulation was combined with mTORi-NB or S6K1i-NB treatment, priming was prevented (**Figure 5B** and **S6B**), indicating that mTOR-S6K1 signaling is required for oxLDL priming.

Subsequently, we performed single-cell RNA sequencing of non-primed (RPMI) and oxLDL-primed adherent monocytes that were subsequently stimulated with LPS. We

identified cells with low *PSAP* expression (blue dots) in the non-primed monocytes, while PSAP expression was high in nearly all monocytes primed with oxLDL (**Figure 5C**). Interestingly, we also observed that the prosaposin protein itself was capable of priming human primary monocytes, as evidenced by the enhanced cytokine production upon re-stimulation with LPS (**Figure 5D**).

To investigate prosaposin's involvement in human atherosclerosis, we obtained carotid plaque specimens from patients undergoing elective endarterectomy, and stained them for prosaposin. We confirmed prosaposin's presence in human plaques and its colocalization with plaque macrophages (**Figure 5E** and **S7A**). We further explored this on a transcriptional level, utilizing single-cell RNA sequencing of 18 human plaques[20].

Here, 14 distinct leukocyte populations were identified, among which four different CD14$^+$CD68$^+$ macrophage subtypes (**Figure 5F**). Interestingly, the highest *PSAP* expression was found in the macrophage populations, with relatively lower expression across the other leukocytes (**Figure 5F**). Given the strong relationship between mTOR signaling and *Psap* expression in mouse plaques, we set out to study this in human atherosclerosis. To this aim, we analyzed transcriptome data from 620 carotid plaques[20]. In these tissues, *PSAP* was highly expressed, as compared to the average expression of a random sample of other genes (**Figure S7B**). Among the 40 genes assigned to the mTOR signaling pathway, we found *PSAP* to correlate with elements of the Ragulator complex (*LAMTOR1*, *LAMTOR2* and *LAMTOR5*), a component of active mTORC1 (**Figures 5G**, **S7C** and **S8A, Table S7**). Furthermore, we found co-expression of *PSAP* and *RPS6*, which provides a link to S6K1 signaling, as S6K1 catalyzes the phosphorylation of ribosomal protein S6, encoded by *RPS6*.

Recently published single-cell transcriptional data from atherosclerotic plaques of mice and humans identified gene signatures of distinct macrophage populations [21,22]. We investigated the relationship of *PSAP* with gene expression related to these previously identified signatures. Interestingly, *APOE*, *APOC1*, *CCL2*, *CTSB*, *CTSD* and *MMP9* displayed the highest co-expression with *PSAP* (**Figure 5H** and **S8B, Table S8**). They were all identified as markers of the same macrophage cluster in human atherosclerosis by Fernandez *et al.* *APOE* and *APOC1* are related to cholesterol uptake and believed to be markers for foam cells. *CCL2, CTSB, CTSD* and *MMP9* are important inflammatory markers and involved in matrix degradation. *CTSB,* encoding for Cathepsin B, was also recognized as one of the downregulated hub genes in our murine plaque transcriptome analysis (**Figure 2C**), and is the molecular target of FMT-CT imaging, which was reduced by mTORi-NB treatment (**Figure 1H**). When we

9
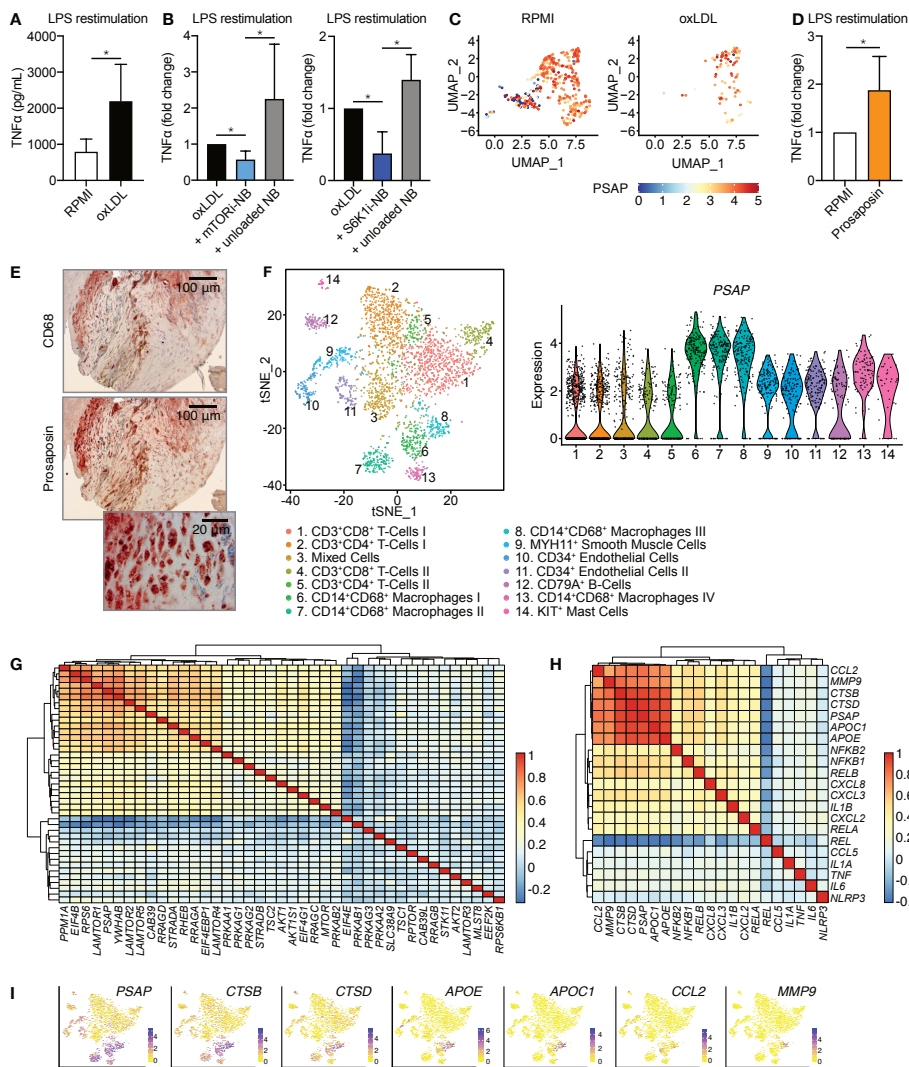
Figure 5. *PSAP* mediates atherosclerotic plaque inflammation in humans. (A-D) Human primary monocytes were incubated with oxidized LDL (oxLDL) or prosaposin for 24 hours. After a 5-day rest, cells were restimulated with LPS. (A) OxLDL amplifies the TNFα production upon LPS stimulation, as measured by ELISA (n=6). (B) When human monocytes are primed with oxLDL, in combination with mTORi-NB or S6K1i-NB, TNFα production is reduced, as compared to unloaded NB or oxLDL only (n=6). (C) After oxLDL priming and LPS restimulation, single cell transcriptome analysis was performed on adherent human monocytes. A UMAP plot shows the different monocyte clusters and *PSAP* expression is shown for each cell (n=3). (D) Human monocytes were primed with prosaposin or RPMI (negative control) for 24 hours. After a 5-day rest, cells were restimulated with LPS and TNFα production was measured by ELISA, (n=5). (E) Representative images of CD68 (top) and prosaposin (middle and bottom) staining on a human carotid endarterectomy sample. Prosaposin is abundantly expressed in the plaque and colocalizes with CD68-positive areas. (F) Single-cell RNA sequencing of human atherosclerotic plaques identifies 14 leukocyte subsets. The highest *PSAP* expression is detected in the four CD14+CD68+ macrophage subsets (n=18). (G,H) Transcriptomic analyses were performed on human atherosclerotic plaques (n=620). Heatmap depicting co-expression of *PSAP* and genes involved in (G) the mTOR signaling pathway or (H) atherosclerotic plaque macrophages, clustered based on co-expression values. (I) Expression of 6 inflammatory genes, as compared to PSAP expression, based on single-cell RNA sequencing, also presented in (F). Bar graphs are presented as mean ± SD. *p<0.05, **p<0.01, ***p<0.001, ****p<0.0001.

evaluated the expression of these six genes in our own single-cell transcriptional data, CTSB and CTSD mostly resembled the cell-specific expression pattern of PSAP, further affirming their connectivity (**Figure 5I**).

Collectively, these data demonstrate that the expression of *PSAP* is related to mTOR signaling and inflammation in human atherosclerotic lesions.

DISCUSSION

Atherosclerosis is a cholesterol-induced inflammatory disease in which monocytes and macrophages are the main protagonists. The mTOR signaling network is fundamental for balancing anabolic and catabolic pathways in response to the nutritional status in all eukaryotic cells and plays a dominant role in regulating inflammatory activity in immune cells. In this study we show that myeloid cell-specific mTOR and S6K1 inhibition rapidly suppresses plaque inflammation in atherosclerotic mice. We identified prosaposin as a mediator of these anti-inflammatory effects and reveal prosaposin's regulating role in immunometabolism. In humans we confirmed high *PSAP* expression in plaque macrophages and found it to be related to mTOR signaling and inflammation.

Prosaposin is the precursor of four similar proteins named saposin A, B, C and D [23,24] and this protein is highly conserved in evolution [19]. Saposins are essential for lysosomal degradation of glycosphingolipids by facilitating the access of the degrading enzymes to their substrates [25]. Deleterious genetic mutations in any of the saposin domains lead to lysosomal storage disease [26]. Besides the intracellular function of prosaposin in lysosomes, the protein is also excreted and can be detected in various body fluids including serum [27]. Concerning hematopoietic cells, prosaposin is predominantly expressed in monocytes and macrophages, and much lower expression is found in lymphocytes [28]. Prosaposin and the individual saposins are known to have specific immunological functions in innate immune cells [14]. Saposins are indispensable for lipid antigen presentation to CD1-restricted T cells, as they mobilize lipids from lysosomal membranes to facilitate their association with CD1d [14]. CD1 lipid antigen presentation is of relevance in infectious diseases such as *Mycobacterium tuberculosis* [29]. Interestingly, CD1 is also important in atherosclerosis, exemplified by the fact that *CD1d⁻/⁻Apoe⁻/⁻* mice, which are incapable of lipid antigen presentation, showed markedly reduced atherosclerosis development [30,31]. Furthermore, prosaposin is related to progranulin, with which it interacts to facilitate its lysosomal

targeting [32]. Progranulin is of importance in the innate immune response and was previously found to be highly expressed in atherosclerotic plaque macrophages [33–35].

In our current study we revealed prosaposin to be an important mediator of the anti-inflammatory effect of mTOR and S6K1 inhibition in plaque macrophages. This may in part be mediated through above mentioned effects on CD1 lipid antigen presentation and/or progranulin. Another mechanism may be prosaposin's central role in sphingolipid metabolism [14]. Sphingolipids are universal building blocks of cell membranes and include ceramide, sphingomyelin and many different forms of glycosphingolipids [36]. Sphingolipid metabolites, particularly ceramide and sphingosine-1-phosphate (S1P), modulate a wide variety of cellular processes involved in inflammation, cell cycle and metabolism [36–38]. Ceramides affect cellular metabolism by inhibiting uptake of amino acids [39,40] and glucose [41], leading to utilization of fatty acids for energy production [38]. Besides this, ceramides influence mitochondrial activity by changing the mitochondrial membrane potential [42], which is required for efficient ATP production through oxidative phosphorylation. Furthermore, the respiratory chain activity can be modified by ceramides [43,44].

The precise role of *PSAP* in human atherosclerosis has not been studied previously. The rapid progress of single-cell technologies, such as single-cell RNA sequencing and CyTOF, aids in unraveling cellular subsets, phenotypes, and also the underlying cellular processes of a complex disease as atherosclerosis. Recently, Fernandez *et al.* defined human plaque macrophage clusters based on their gene expression signatures. In their data, *PSAP* appeared in one of their clusters which corroborates our data from both mice and human atherosclerosis [22]. Similar to the observation made by Fernandez *et al.*, we show *PSAP* to be coexpressed with other genes known to play an important role in plaque inflammation, namely *APOE*, *APOC1*, *CCL2*, *CTSB*, *CTSD* and *MMP9*.

In this study we reveal the role of prosaposin in atherosclerosis in both mice and humans. This invites us to reflect on the possibilities to target prosaposin or the individual saposin domains for the treatment of atherosclerosis. RNA interference with siRNA could be a way to achieve this, as we also applied in our current study. siRNA therapy is highly specific to its target. Yet, the off-target effects on *PSAP* suppression in other tissues could be a limitation. This may be overcome by targeting the therapy specifically to myeloid cells [45]. This can be accomplished by nanotherapeutic siRNA delivery as we have utilized in our current study [46]. Another way of *PSAP*-targeted treatment could be the application of small molecules binding to prosaposin or the saposin domains. To our knowledge no specific small molecule inhibi-

tor has been developed for this purpose. However, from literature we found that the anti-malarial drug hydroxychloroquine binds to saposin B [47]. Hydroxychloroquine is an immunomodulating drug used to treat rheumatoid arthritis and systemic lupus erythematosus (SLE), and recent studies showed anti-atherosclerotic effects in SLE patients [48,49]. Another potential strategy may be to interfere with sphingolipid signaling. S1P receptor 1 modulators and agonists are currently approved for the treatment multiple sclerosis, an auto-immune disease of the central nervous system in which macrophages play a central role [50]. S1P receptor 1 modulators and agonists were also observed to reduce atherosclerosis in experimental studies by modulating macrophage function [51,52].

Collectively, our findings advance several concepts. First, we show that mTOR and S6K1 inhibition in myeloid cells rapidly reduces plaque inflammation. Second, we found prosaposin to be an important mediator of these anti-inflammatory effects, which likely relates to prosaposin's effect on cell metabolism. Third, we show that prosaposin is associated with plaque inflammation in human atherosclerosis. Our data identify prosaposin and the individual saposin domains as potential therapeutic targets for the treatment of atherosclerosis.

9

REFERENCES

1. Tabas, I. & Lichtman, A. H. Monocyte-Macrophages and T Cells in Atherosclerosis. *Immunity* **47**, 621–634 (2017).

2. O'Neill, L. A. J., Kishton, R. J. & Rathmell, J. A guide to immunometabolism for immunologists. *Nat. Rev. Immunol.* **16**, 553–565 (2016).

3. Ketelhuth, D. F. J. *et al.* Immunometabolism and atherosclerosis: Perspectives and clinical significance: A position paper from the Working Group on Atherosclerosis and Vascular Biology of the European Society of Cardiology. *Cardiovasc. Res.* **115**, 1385–1392 (2019).

4. Koelwyn, G. J., Corr, E. M., Erbay, E. & Moore, K. J. Regulation of macrophage immunometabolism in atherosclerosis. *Nat. Immunol.* **19**, 526–537 (2018).

5. Tomas, L. *et al.* Altered metabolism distinguishes high-risk from stable carotid atherosclerotic plaques. *Eur. Heart J.* **39**, 2301–2310 (2018).

6. Weichhart, T., Hengstschläger, M. & Linke, M. Regulation of innate immune cell function by mTOR. *Nat. Rev. Immunol.* **15**, 599–614 (2015).

7. Saxton, R. A. & Sabatini, D. M. mTOR Signaling in Growth, Metabolism, and Disease. *Cell* **168**, 960–976 (2017).

8. Duivenvoorden, R. *et al.* A statin-loaded reconstituted high-density lipoprotein nanoparticle inhibits atherosclerotic plaque inflammation. *Nat. Commun.* **5**, 3065 (2014).

9. Lameijer, M. *et al.* Efficacy and safety assessment of a TRAF6-targeted nanoimmunotherapy in atherosclerotic mice and non-human primates. *Nat. Biomed. Eng.* **2**, 279–292 (2018).

10. Pearce, L. R. *et al.* Characterization of PF-4708671, a novel and highly specific inhibitor of p70 ribosomal S6 kinase (S6K1). *Biochem. J.* **431**, 245–255 (2010).

11. Nahrendorf, M. *et al.* Hybrid in vivo FMT-CT imaging of protease activity in atherosclerosis with customized nanosensors. *Arterioscler. Thromb. Vasc. Biol.* **29**, 1444–1451 (2009).

12. Razani, B. *et al.* Autophagy Links Inflammasomes to Atherosclerotic Progression. *Cell Metab.* **15**, 534–544 (2012).

13. Langfelder, P., Mischel, P. S. & Horvath, S. When Is Hub Gene Selection Better than Standard Meta-Analysis? *PLoS One* **8**, e61505 (2013).

14. Darmoise, A., Maschmeyer, P. & Winau, F. *The immunological functions of saposins*. *Advances in Immunology* **105**, (Elsevier Inc., 2010).

15. Keating, S. T. *et al.* Rewiring of glucose metabolism defines trained immunity induced by oxidized low-density lipoprotein. *J. Mol. Med.* (2020). doi:10.1007/s00109-020-01915-w

16. Kulkarni, J. A., Witzigmann, D., Chen, S., Cullis, P. R. & van der Meel, R. Lipid Nanoparticle Technology for Clinical Translation of siRNA Therapeutics. *Acc. Chem. Res.* **52**, 2435–2444 (2019).

17. Van Eck, M. *et al.* Bone Marrow Transplantation in Apolipoprotein E–Deficient Mice. *Arterioscler. Thromb. Vasc. Biol.* **17**, 3117–3126 (1997).

18. Thomas, G., Tacke, R., Hedrick, C. C. & Hanna, R. N. Nonclassical Patrolling Monocyte Function in the Vasculature. *Arterioscler. Thromb. Vasc. Biol.* **35**, 1306–1316 (2015).

19. Hazkani-Covo, E., Altman, N., Horowitz, M. & Graur, D. The Evolutionary History of Prosaposin: Two Successive Tandem-Duplication Events Gave Rise to the Four Saposin Domains in Vertebrates. *J. Mol. Evol.* **54**, 30–34 (2002).

20. Depuydt, M. A. C. *et al.* Microanatomy of the Human Atherosclerotic Plaque

by Single-Cell Transcriptomics. *Circ. Res.* **127**, 1437–1455 (2020).

21. Willemsen, L. & de Winther, M. P. Macrophage subsets in atherosclerosis as defined by single-cell technologies. *J. Pathol.* **250**, 705–714 (2020).

22. Fernandez, D. M. *et al.* Single-cell immune landscape of human atherosclerotic plaques. *Nat. Med.* **25**, 1576–1588 (2019).

23. Fürst, W., Machleidt, W. & Sandhoff, K. The precursor of sulfatide activator protein is processed to three different proteins. *Biol. Chem. Hoppe. Seyler.* **369**, 317–28 (1988).

24. O'Brien, J. S. *et al.* Coding of two sphingolipid activator proteins (SAP-1 and SAP-2) by same genetic locus. *Science (80-.).* **241**, 1098–101 (1988).

25. Sandhoff, K. & Kolter, T. Biochemistry of glycosphingolipid degradation. *Clin. Chim. Acta.* **266**, 51–61 (1997).

26. Ferreira, C. R. & Gahl, W. A. Lysosomal storage diseases. *Transl. Sci. Rare Dis.* **2**, 1–71 (2017).

27. Hineno, T. *et al.* Secretion of sphingolipid hydrolase activator precursor, prosaposin. *Biochem. Biophys. Res. Commun.* **176**, 668–674 (1991).

28. Uhlen, M. *et al.* Tissue-based map of the human proteome. *Science (80-.).* **347**, 1260419–1260419 (2015).

29. Beckman, E. M. *et al.* Recognition of a lipid antigen by CD1-restricted αβ+ T cells. *Nature* **372**, 691–694 (1994).

30. Getz, G. S. & Reardon, C. A. Natural killer T cells in atherosclerosis. *Nat. Rev. Cardiol.* **14**, 304–314 (2017).

31. Tupin, E. *et al.* CD1d-dependent Activation of NKT Cells Aggravates Atherosclerosis. *J. Exp. Med.* **199**, 417–422 (2004).

32. Zhou, X. *et al.* Prosaposin facilitates sortilin-independent lysosomal trafficking of progranulin. *J. Cell Biol.* **210**, 991–1002 (2015).

33. He, Z. & Bateman, A. Progranulin (granulin-epithelin precursor, PC-cell-derived growth factor, acrogranin) mediates tissue repair and tumorigenesis. *J. Mol. Med.* **81**, 600–612 (2003).

34. Kawase, R. *et al.* Deletion of progranulin exacerbates atherosclerosis in ApoE knockout mice. *Cardiovasc. Res.* **100**, 125–133 (2013).

35. Yin, F. *et al.* Exaggerated inflammation, impaired host defense, and neuropathology in progranulin-deficient mice. *J. Exp. Med.* **207**, 117–128 (2010).

36. MacEyka, M. & Spiegel, S. Sphingolipid metabolites in inflammatory disease. *Nature* **510**, 58–67 (2014).

37. Hannun, Y. A. & Obeid, L. M. Sphingolipids and their metabolism in physiology and disease. *Nat. Rev. Mol. Cell Biol.* **19**, 175–191 (2018).

38. Summers, S. A., Chaurasia, B. & Holland, W. L. Metabolic Messengers: ceramides. *Nat. Metab.* **1**, 1051–1058 (2019).

39. Guenther, G. G. *et al.* Ceramide starves cells to death by downregulating nutrient transporter proteins. *Proc. Natl. Acad. Sci. U. S. A.* **105**, 17402–17407 (2008).

40. Hyde, R., Hajduch, E., Powell, D. J., Taylor, P. M. & Hundal, H. S. Ceramide down-regulates System A amino acid transport and protein synthesis in rat skeletal muscle cells. *FASEB J.* **19**, 1–24 (2005).

41. Summers, S. A., Garza, L. A., Zhou, H. & Birnbaum, M. J. Regulation of Insulin-Stimulated Glucose Transporter GLUT4 Translocation and Akt Kinase Activity by Ceramide. *Mol. Cell. Biol.* **18**, 5457–5464 (1998).

42. Arora, A. S., Jones, B. J., Patel, T. C., Bronk, S. F. & Gores, G. J. Ceramide induces hepatocyte cell death through disruption of mitochondrial function

9

in the rat. *Hepatology* **25**, 958–963 (1997).

43. Kogot-Levin, A. & Saada, A. Ceramide and the mitochondrial respiratory chain. *Biochimie* **100**, 88–94 (2014).

44. Zigdon, H. *et al.* Ablation of Ceramide Synthase 2 Causes Chronic Oxidative Stress Due to Disruption of the Mitochondrial Respiratory Chain. *J. Biol. Chem.* **288**, 4947–4956 (2013).

45. Novobrantseva, T. I. *et al.* Systemic RNAi-mediated Gene Silencing in Non-human Primate and Rodent Myeloid Cells. *Mol. Ther. - Nucleic Acids* **1**, e4 (2012).

46. Duivenvoorden, R. *et al.* Nanoimmunotherapy to treat ischaemic heart disease. *Nat. Rev. Cardiol.* **16**, 21–32 (2019).

47. Tinklepaugh, J. *et al.* Exploring the multiligand binding specificity of saposin B reveals two binding sites. *ACS Omega* **2**, 7141–7145 (2017).

48. Schrezenmeier, E. & Dörner, T. Mechanisms of action of hydroxychloroquine and chloroquine: implications for rheumatology. *Nat. Rev. Rheumatol.* **16**, 155–166 (2020).

49. Floris, A. *et al.* Protective effects of hydroxychloroquine against accelerated atherosclerosis in systemic lupus erythematosus. *Mediators Inflamm.* **2018**, (2018).

50. Derfuss, T. *et al.* Advances in oral immunomodulating therapies in relapsing multiple sclerosis. *Lancet. Neurol.* **19**, 336–347 (2020).

51. Nofer, J.-R. *et al.* FTY720, a Synthetic Sphingosine 1 Phosphate Analogue, Inhibits Development of Atherosclerosis in Low-Density Lipoprotein Receptor–Deficient Mice. *Circulation* **115**, 501–508 (2007).

52. Potì, F. *et al.* KRP-203, Sphingosine 1-Phosphate Receptor Type 1 Agonist, Ameliorates Atherosclerosis in LDL-R −/− Mice. *Arterioscler. Thromb. Vasc. Biol.* **33**, 1505–1512 (2013).

53. World Medical Association. World Medical Association Declaration of Helsinki: Ethical Principles for Medical Research Involving Human Subjects. *JAMA* **310**, 2191–2194 (2013).

54. Jonas, A. Reconstitution of high-density lipoproteins. *Methods Enzymol.* **128**, 553–82 (1986).

55. Braza, M. S. *et al.* Inhibiting Inflammation with Myeloid Cell-Specific Nanobiologics Promotes Organ Transplant Acceptance. *Immunity* **49**, 819-828.e6 (2018).

56. van der Laan, S. W. *et al.* Variants in ALOX5, ALOX5AP and LTA4H are not associated with atherosclerotic plaque phenotypes: The Athero-Express Genomics Study. *Atherosclerosis* **239**, 528–538 (2015).

57. Muraro, M. J. *et al.* A Single-Cell Transcriptome Atlas of the Human Pancreas. *Cell Syst.* **3**, 385-394.e3 (2016).

58. Butler, A., Hoffman, P., Smibert, P., Papalexi, E. & Satija, R. Integrating single-cell transcriptomic data across different conditions, technologies, and species. *Nat. Biotechnol.* **36**, 411–420 (2018).

59. Martens, J. H. A. & Stunnenberg, H. G. BLUEPRINT: mapping human blood cell epigenomes. *Haematologica* **98**, 1487–1489 (2013).

60. Aran, D. *et al.* Reference-based analysis of lung single-cell sequencing reveals a transitional profibrotic macrophage. *Nat. Immunol.* **20**, 163–172 (2019).

61. B. Langmead, S. L. Salzberg, Fast gapped-read alignment with Bowtie 2, *Nat. Methods* **9**, 357–359 (2012).

62. S. Anders, P. T. Pyl, W. Huber, HTSeq-A Python framework to work with high-throughput sequencing data, *Bioinformatics* **31**, 166–169 (2015).

63. J. M. Mudge, J. Harrow, Creating reference gene annotation for the mouse C57BL6/J genome assembly, *Mamm. Genome* **26**, 366–378 (2015).

64. M. E. Ritchie, B. Phipson, D. Wu, Y. Hu, C. W. Law, W. Shi, G. K. Smyth, limma powers differential expression analyses for RNA-sequencing and microarray studies., *Nucleic Acids Res.* **43**, e47 (2015).

65. B. Zhang, S. Horvath, A General Framework for Weighted Gene Co-Expression Network Analysis, *Stat. Appl. Genet. Mol. Biol.* **4** (2005), doi:10.2202/1544-6115.1128.

66. P. Shannon, A. Markiel, O. Ozier, N. S. Baliga, J. T. Wang, D. Ramage, N. Amin, B. Schwikowski, T. Ideker, Cytoscape: a software environment for integrated models of biomolecular interaction networks., *Genome Res.* **13**, 2498–504 (2003).

67. W.-M. Song, B. Zhang, E. Wang, Ed. Multiscale Embedded Gene Co-expression Network Analysis, *PLOS Comput. Biol.* **11**, e1004574 (2015).

68. S. Bekkering, B. A. Blok, L. A. B. Joosten, N. P. Riksen, R. Van Crevel, M. G. Netea, In Vitro Experimental Model of Trained Innate Immunity in Human, *Clin. vaccine Immunol.* **23**, 926–934 (2016).

69. L. J. H. Van Tits, R. Stienstra, P. L. Van Lent, M. G. Netea, L. A. B. Joosten, A. F. H. Stalenhoef, Oxidized LDL enhances pro-inflammatory responses of alternatively activated M2 macrophages : A crucial role for Krüppel-like factor 2, *Atherosclerosis* **214**, 345–349 (2011).

70. T. Stuart, A. Butler, P. Hoffman, C. Hafemeister, E. Papalexi, W. M. Mauck, Y. Hao, M. Stoeckius, P. Smibert, R. Satija, Comprehensive Integration of Single-Cell Data., *Cell* **177**, 1888-1902.e21 (2019).

71. T. Hashimshony, F. Wagner, N. Sher, I. Yanai, CEL-Seq: Single-Cell RNA-Seq by Multiplexed Linear Amplification, *Cell Rep.* **2**, 666–673 (2012).

72. T. Hashimshony, N. Senderovich, G. Avital, A. Klochendler, Y. de Leeuw, L. Anavy, D. Gennert, S. Li, K. J. Livak, O. Rozenblatt-Rosen, Y. Dor, A. Regev, I. Yanai, CEL-Seq2: sensitive highly-multiplexed single-cell RNA-Seq, *Genome Biol.* **17**, 77 (2016).

73. M. A. M. M. Ferraz, H. S. Rho, D. Hemerich, H. W. W. Henning, H. T. A. van Tol, M. Hölker, U. Besenfelder, M. Mokry, P. L. A. M. Vos, T. A. E. Stout, S. Le Gac, B. M. Gadella, An oviduct-on-a-chip provides an enhanced in vitro environment for zygote genome reprogramming, *Nat. Commun.* **9**, 4934 (2018).

74. H. Li, R. Durbin, Fast and accurate short read alignment with Burrows-Wheeler transform, *Bioinformatics* **25**, 1754–1760 (2009).

75. M. I. Love, W. Huber, S. Anders, Moderated estimation of fold change and dispersion for RNA-seq data with DESeq2, *Genome Biol.* **15**, 550 (2014).

9

MATERIALS AND METHODS

Study design

We designed and formulated two myeloid cell-specific nanobiologics to selectively inhibit mTOR signaling pathway. We treated Apoe$^{-/-}$ mice with these nanobiologics for one week and employed flow cytometry and histology to study the systemic immune status and plaque inflammation (n=20/group). By investigating transcriptome modifications, we identified Psap, a gene encoding for prosaposin, to be closely related with mTOR signaling (n=10/group). Subsequently, Psap siRNA lipid nanoparticles were designed and formulated to study the influence of Psap's on immune cell metabolism. Here we used bone marrow derived macrophages and a metabolic flux assay (n=10/condition). To study the direct effects of Psap on atherosclerotic inflammation, we transplanted Psap$^{-/-}$ or Psap$^{+/+}$ bone marrow in lethally irradiated Ldlr$^{-/-}$ mice and again studied the systemic immune status and plaque inflammation (n=20/group). Finally, we corroborated our findings in human monocytes through in vitro assays (n=6), single cell RNA sequencing (n=3) and in human atherosclerotic plaque specimens through histology (n=4), single cell RNA sequencing (n=18) and bulk RNA sequencing (n=620).

Mice

Female Apoe$^{-/-}$ mice (B6.129P2-Apoe^{tm1Unc}/J), female Ldlr$^{-/-}$ mice (B6.129S7-Ldlr^{tm1Her}/J) and male and female Psap$^{+/-}$ mice (B6.129P2-Psap^{tm1Suz}/J) were purchased from The Jackson Laboratory. Eight-week-old Apoe$^{-/-}$ mice were fed a Western diet (0.2% weight cholesterol; 15.2% kcal protein, 42.7% kcal carbohydrate, 42.0% kcal fat; Harlan TD. 88137) for 12 weeks. Male and female Psap$^{+/-}$ mice were bred to obtain Psap$^{-/-}$ and Psap$^{+/+}$ mice. After bone marrow transplantation and reconstitution, Ldlr$^{-/-}$ mice were fed a Western diet for 11 weeks. Animal care and procedures were based on an approved institutional protocol from Icahn School of Medicine at Mount Sinai.

In vitro experiments were performed on bone marrow-derived macrophages (BMD-Ms). BMDMs were cultured in cell culture dishes, in Roswell Park Memorial Institute medium (RPMI) supplemented with 10% fetal bovine serum, 2mM L-Glutamine,100 U/mL Penicillin-Streptomycin and 15% L929-cell-conditioned medium. All cells were incubated at 37 °C in a 5% CO_2 atmosphere.

Human subjects

For in vitro studies on human monocytes, buffy coats from healthy donors were obtained after written informed consent (Sanquin blood bank, Nijmegen, The Netherlands). For histologic analysis, human atherosclerotic plaque samples were

obtained from four patients. All four patients had an indication for carotid endarterectomy. Gender of the included subjects for both studies is known, although gender association cannot be analyzed due to small group sizes. Subject allocation to groups is not applicable.

For bulk RNA-seq and single-cell RNA-seq analysis of human carotid atherosclerotic plaques from the Athero-Express Biobank Study, research was executed according to the principles of the Declaration of Helsinki and its later amendments [53] all patients provided informed consent and the study was approved by the medical ethics committee of the UMC Utrecht.

Synthesis of nanobiologics

Nanobiologic formulations were synthesized according to previously published methods[54,55]. For mTORi-NB, the mTORC1-complex inhibitor rapamycin (3 mg, 3.3 µmol), was combined with 1-myristoyl-2-hydroxy-sn-glycero-phosphocholine (MHPC) (6 mg, 12.8 µmol) and 1,2-dimyristoyl-sn-glycero-3-phosphocholine (DMPC) (18 mg, 26.6 µmol) (Avanti Polar Lipids). For S6K1i-NB, the S6K1 inhibitor PF-4708671 (1.5 mg, 4.6 µmol) was combined with 1-palmitoyl-2-oleoyl-sn-glycero-3-phosphocholine (POPC) (18 mg, 23.7 µmol) and 1-palmitoyl-2-hydroxy-sn-glycero-3-phosphocholine (PHPC) (6 mg, 12.1 µmol). The inhibitors and lipids were dissolved in methanol and chloroform, mixed, and then dried in a vacuum, yielding a thin lipid film. A PBS solution containing human apolipoprotein A1 (APOA1) (4.8 mg in 5 mL PBS) was added to the lipid film. The mixture was incubated in an ice-cold sonication bath for 15-30 minutes. Subsequently, the solution was sonicated using a tip sonicator at 0 °C for 20 minutes to form APOA1 based nanobiologics. The obtained solution was concentrated by centrifugal filtration using a 100k MWCO Vivaspin tube at 3000 rpm to obtain a volume of ~1 mL, and then washed twice with fresh PBS (5 mL). The concentrated solution (~1 mL) was filtered through a 0.22 µm PES syringe filter to obtain the final nanobiologic solution. For targeting and biodistribution experiments, analogs of mTORi-NB and S6K1i-NB were prepared by incorporating the fluorescent dyes DiR or DiO (Invitrogen).

Nanobiologic treatment

Twenty-week-old Apoe^{-/-} received either PBS, unloaded nanobiologics, mTORi-NB (mTORi at 5 mg/kg), or S6K1i-NB (S6K1i at 5 mg/kg) through lateral tail vein injections. Mice were treated with 4 injections over 7 days while being kept on a Western diet. For the targeting and biodistribution experiments, mice received a single intravenous injection. All animals were euthanized 24 hours after the last injection.

9

Histology and immunohistochemistry

For Mac3, CD68 and prosaposin staining, tissues were fixed in formalin, embedded in paraffin and sectioned into 4 µm slices. To perform immunohistochemical staining, mouse aortic roots and human carotid endarterectomy (CEA) sections were deparaffinized, blocked using 4% FCS in PBS for 30 minutes, and incubated in antigen-retrieval solution (DAKO) at 95 °C for 10 minutes. Mouse aortic root sections were immunolabeled with rat anti-mouse Mac3 monoclonal antibody (1:30, BD Biosciences). CEA samples were stained for macrophages using a donkey anti-mouse CD68 primary antibody (1:300, Abcam) in combination with a biotinylated donkey anti-mouse secondary antibody (1:300; Jackson ImmunoResearch). Both mouse aortic roots and CEA samples were stained for prosaposin using a rabbit anti-human prosaposin primary antibody (1:500, Abcam) in combination with a biotinylated goat anti-rabbit secondary antibody (1:300, DAKO). Antibody staining was visualized by either Immpact AMEC red (Vectorlabs) or diaminobenzidine (DAB). Sections were analyzed using a Leica DM6000 microscope (Leica Microsystems) or the VENTANA iScan HT slide scanner (Ventana).

Aortic root samples from $Ldlr^{-/-}$ mice were harvested, embedded in Tissue-Tek O.C.T., and sectioned into 7 µm slices. To acquire lesion volume sections were collected starting at the beginning of the artic root until the aortic valves were no longer visible. After staining with H&E the lesion area was measured in intervals of 84 µm using Adobe Photoshop. The generated lesion area was plotted against the distance from the artic root after which the lesion volume was obtained by calculating the area under the curve. Sirius red staining was used for the analysis of collagen content.

Near-infrared fluorescence imaging

Mice received a single intravenous injection with DiR (0.5 mg/kg) labeled mTORi-NB (5 mg/kg) or S6K1i-NB (5 mg/kg). Liver, spleen, lung, kidneys, heart and muscle tissue were collected for NIRF imaging. Fluorescent images were acquired using an IVIS 200 system (Xenogen), with a 2 second exposure time, using a 745 nm excitation filter and an 820 nm emission filter. ROIs were drawn on each tissue with software provided by the vendor, after which quantitative analyses were performed using the average radiant efficiency within these ROIs.

Preparation of single-cell suspensions for flow cytometry

Blood was collected by cardiac puncture and mice were subsequently perfused with 20 mL cold PBS. Spleen and femurs were harvested. The aorta, from aortic root to the iliac bifurcation, was gently cleaned of fat and collected. The aorta was digested

using an enzymatic digestion solution containing liberase TH (4 U/mL) (Roche), deoxyribonuclease (DNase) I (40 U/mL) (Sigma-Aldrich), and hyaluronidase (60 U/mL) (Sigma-Aldrich) in PBS at 37 °C for 60 minutes. Cells were filtered through a 70 μm cell strainer and washed with serum-containing media. Blood was incubated with lysis buffer for 4 minutes and washed with serum-containing media. Spleens were mashed, filtered through a 70 μm cell strainer, incubated with lysis buffer for 4 minutes and washed with serum-containing media. Bone marrow was flushed out of the femur with PBS, filtered through a 70 μm cell strainer, incubated with lysis buffer for 30 seconds and washed with serum-containing media.

Flow cytometry

Single-cell suspensions from the aorta, blood, spleen and bone marrow were stained with the following monoclonal antibodies: anti-CD11b (clone M1/70), anti-F4/80 (clone BM8); anti-CD11c (clone N418), anti-CD45 (clone 30-F11), anti-Ly6C (clone AL-21), and a lineage antibody cocktail (Lin) containing anti-CD90.2 (clone 53-2.1), anti-Ter119 (clone TER119), anti-NK1.1 (clone PK136), anti-CD49b (clone DX5), anti-CD45R (clone RA3-6B2) and anti-Ly6G (clone 1A8). Hematopoietic stem and pro-genitor cells were identified by staining bone marrow cells with: anti-CD117 (c-Kit, clone 2B8), anti-Sca1 (clone E13-161.7), anti-CD48 (clone HM48-1), anti-CD150 (clone TC15-12F12.2) and a commercially available lineage antibody cocktail containing anti-CD3e (clone 500A2), anti-CD11b (clone M1/70), anti-CD45R/B220 (clone RA3-6B2), anti-Ly-76 (clone TER-119), anti Ly6C and anti-Ly6G (both clone RB6-8C5).The contribution of newly made cells to different populations was determined by *in vivo* labeling with 5-Bromo-2'-deoxy-uridine (BrdU). Mice were injected with 1 mg BrdU 24 hours before sacrifice. BrdU flow kits were used according to the manufacturer's protocol. Data were acquired on a BD LSRII and a BD LSRFortessa flow cytometer (BD Biosciences). DiO signal was detected in the FITC channel. Counting beads were added to calculate absolute cell numbers. Data were analyzed using FlowJo v10.0.7 (Tree Star).

Fluorescence molecular tomography with CT

After nanobiologic treatment, mice were injected with 5 nanomoles of pan-cathepsin protease sensor (ProSense 680, PerkinElmer, Cat no. NEV10003). Twenty-four hours later, animals were placed in a custom build cartridge and sedated during imaging with continuous isoflurane administration as described previously[10]. Animals were first scanned using a high-resolution CT scanner (Inveon PET-CT, Siemens), with a continuous infusion of CT-contrast agent (isovue-370, Bracco Diagnostics) at a rate of 55 μL/min through a tail vein catheter. Animals were subsequently scanned using an FMT scanner (PerkinElmer) in the same cartridge. The CT X-ray source with an

exposure time of 425 milliseconds over 360 projections, was operated at 80 kVp and 500 μA. CT images were reconstructed using a modified Feldkamp cone beam reconstruction algorithm (COBRA, Exxim Inc.) Contrast-enhanced high-resolution CT images were used to localize the aortic root, which was used to guide the placement of the volume of interest for the quantitative FMT protease activity map. Image fusion relied on fiducial markers built into the imaging cartridge. Image fusion and analysis were performed using OsiriX v.6.5.2 (The Osirix Foundation, Geneva).

Laser capture microdissection

Laser capture microdissection was performed on 24 aortic root sections (6 μm). Frozen sections were dehydrated in graded ethanol solutions (70% twice, 95% twice, 100% once), washed with diethylpyrocarbonate (DEPC)-treated water, stained with Mayer's H&E and cleared in xylene. For every 8 sections, 1 section was used for CD68 staining (Abd Serotec, 1:250 dilution), which was used to guide the laser capture microdissection. CD68-rich areas within the plaques were identified and collected using an ArcturusXT LCM System.

RNA sequencing of murine plaque macrophages

The CD68^{+} cells collected by laser capture microdissection were used for RNA isolation (PicoPure RNA Isolation Kit, Arcturus) and subsequent RNA amplification and cDNA preparation according to the manufacturer's protocols (Ovation Pico WTA System, NuGEN). The quality and concentration of the collected samples were measured using an Agilent 2100 Bioanalyzer. For RNA sequencing, pair-end libraries were prepared and validated. The purity, fragment size, yield, and concentration were determined. During cluster generation, the library molecules were hybridized onto an Illumina flow cell. Subsequently, the hybridized molecules were amplified using bridge amplification, resulting in a heterogeneous population of clusters. The data set was obtained using an Illumina HiSeq 2500 sequencer.

RNA sequencing analysis of murine plaque macrophages

For RNA sequencing analysis of CD68^{+} cells isolated from the murine aortic plaque, the pair-ended sequencing reads were aligned to human genome hg19 using TopHat aligner (bowtie2)[61]. Next, HTSeq[62] was used to quantify the gene expression at the gene level based on GENCODE gene model release 22[63]. Gene expression raw read counts were normalized as counts per million using trimmed mean of M-values normalization method to adjust for sequencing library size difference among samples. DEGs between drug treatments and control were identified using the Bioconductor package limma[64]. In order to correct the multiple testing problem, limma was used to calculate t-statistics by permuting sample labels. This procedure was repeated

1,000 times to obtain a null t-statistic distribution for estimating the false discovery rate (FDR) values of all genes. The DEGs of cells isolated from the aortic plaques were identified using a cut-off at an FDR of less than 0.05. A WGCNA was constructed to identify groups of genes (modules) involved in various activated pathways following a previous described algorithm[65]. In short, Pearson correlations were computed between each pair of genes yielding a similarity (correlation) matrix (sij). Subsequently a power function (aij = Power (sij, β) ≡ | sij | β), was used to transform the similarity matrix into an adjacency matrix A [aij], where aij is the strength of a connection between two nodes (genes) i and j in each module. For all genes the connectivity (k) was determined by taking the sum of their connection strengths with all other genes in the network. The parameter was chosen by using the scale-free topology criterion, such that the resulting network connectivity distribution approximated scale-free topology. The adjacency matrix was then used to define a measure of node dissimilarity, based on the TOM. The module subnetworks were visualized using MEGENA and cytoscape[66,67]. To identify gene modules, we performed hierarchical clustering on the TOM. Modules were analyzed with the online annotation tool DAVID.

Bone marrow transplantation

Nine-week-old Ldlr$^{-/-}$ mice were lethally irradiated (2x 600 cGy). Subsequently, bone marrow cells were harvested from 3-week old Psap$^{-/-}$ and Psap$^{+/+}$ mice and transplanted in Ldlr$^{-/-}$ recipients. Mice were kept on polymyxin B sulfate/neomycin, administered through drinking water, for 6 weeks.

siRNA nanotherapeutic formulation and analysis

Psap siRNA (sequence: 5'- rArUrA rArGrU rUrUrU rCrUrG rArGrC rUrGrA rUrUrG rUrCA A -3' and 5'- rUrUrG rArCrA rArUrC rArGrC rUrCrA rGrArA rArArC rUrUrA rUrUrC -3') was purchased from Integrated DNA Technologies. SiRNA (0.176 mg, 10 nmol) was dissolved in nuclease free duplex buffer (7.65 µL), Milli-Q water (3.156 mL), and NaOAc buffer (1.056 mL, 25 mM, pH 4.0). Separately, an ethanol solution (2 mL) containing DLin-MC3-DMA (5.84 mg, 9.10 µmol), DSPC (1.59 mg, 2.01 µmol), cholesterol (3.30 mg, 8.54 µmol), and PEG-DSG (1.31 mg, 0.50 µmol) was created. The siRNA and lipid solutions were microfluidically mixed using BS-2000 microfluidic pumps (Braintree) and a T-junction (made inhouse from PEEK HPLC tubing, details are available on request) (injecting 3.00 mL of siRNA solution at 15.0 mL/min and 1.00 mL lipid solution at 5.01 mL/min). Directly afterwards, the solution was dialyzed (10.000 MWCO) against PBS (400 mL) at 4 °C for 2 days; PBS was refreshed twice during this period. The crude nanotherapeutics were filtered using a 0.2 µm PES syringe filter and concentrated using centrifugal filtration (Vivaspin, 100 kDa MWCO, 4000

rpm, 4 °C). The obtained nanoparticles had a mean size of approximately 32 nm, as determined by dynamic light scattering.

To determine siRNA recovery and entrapment, PBS or nanotherapeutics (50 µL) were mixed with TE buffer (50 µL), in a 96 well plate. Separately, PBS or nanotherapeutics were mixed with TE buffer containing 2% Triton X-100 (50 µL). Lastly, an identical NaOAc buffered siRNA solution as used to formulate the nanotherapeutics was diluted with PBS to obtain siRNA calibrants (0, 8, 16, 32, 40 µg/mL, 50 µL each) which were subsequently mixed with TE buffer containing 2% Triton X-100 (50 µL). The 96 well plate was incubated at 37 °C for 10 minutes. QuantIT RiboGreen was diluted 100x with TE buffer and 100 µL added to each well. Fluorescence intensity was measured directly after (excitation/emission = 490/530 nm). The fluorescent intensities of the respective PBS samples were regarded as background and subtracted from all other samples.

The samples treated with TE buffer will only show the amount of siRNA present in the sample that is not incorporated in the nanotherapeutics. In contrast, the samples treated with TE buffer containing 2% Triton X-100 will show the total amount of siRNA in the sample. *Recovery* = 100% * amount of siRNA found in the sample / amount of siRNA used to formulate the nanotherapeutics. *Entrapment* = 100% * fraction of siRNA in the sample that is inside the nanotherapeutics.

Metabolic extracellular flux analysis

BMDMs were plated at 2.5-5.0 x10^4 cells/well in an XF-96-cell culture plate (Seahorse Bioscience) and left to adhere. BMDMs were incubated with mTORi (20µM), S6K1i (20µM) or DMSO (control) for 16 hours. In a separate assay BMDMs were incubated with Psap siRNA-LNPs (0.5 µg/mL), Ctrl SiRNA-LNPs (0.5 µg/mL) or PBS for 24 hours. The extracellular acidification rate (ECAR) and oxygen consumption rate (OCR) in response to glucose (10 mM), oligomycin (OM, 1.5 µM), carbonyl cyanide 4-(trifluoromethoxy)phenylhydrazone (FCCP, 1.5 µM), and rotenone (ROT, 1.25 µM) + antimycin A (AA, 2.5 µM) injections were measured using a Seahorse XFe96 Analyzer (Agilent). Upon completion, DNA content was measured with CyQuant to compensate for differences in cell numbers. The maximal glycolytic capacity was determined by the difference in ECAR between baseline and FCCP stimulated cells. The maximal respiratory capacity was calculated using the difference in OCR between FCCP and Rot/AA stimulated cells.

Human PBMC and monocyte isolation

PBMC isolation was performed by dilution of blood in pyrogen-free PBS and differential density centrifugation over Ficoll-Paque. Cells were washed three times in PBS. Percoll isolation of monocytes was performed as previously described. Briefly, $150\text{-}200\text{x}10^6$ PBMCs were layered on top of a hyper-osmotic Percoll solution (48.5% Percoll, 41.5% sterile H_2O, 0.16M filter sterilized NaCl) and centrifuged for 15 minutes at 580 g. The interphase layer was isolated and cells were washed once with cold PBS. Cells were resuspended in RPMI culture medium supplemented with 50 μg/ml gentamicin, 2 mM glutamax, and 1 mM pyruvate and counted using a Beckman Coulter counter. An extra purification step was added by adhering Percoll isolated monocytes to polystyrene flat bottom plates (Corning, NY, USA) for 1 hour at 37 °C; subsequently a washing step with warm PBS was performed to yield maximal purity. This increases purity to only 3% T cell contamination as previously described[68].

Preparation of oxidized LDL

LDL was isolated using KBr-density gradient ultracentrifugation from serum from healthy volunteers. Plasma density was adjusted to ρ=1.100 g/mL with KBr. The samples were centrifuged for 22h at 32.000 rpm in a SW41 Ti rotor. Oxidized LDL was prepared by incubation of LDL with 20 μmol $CuSO_4$/L for 15 hours at 37 °C in a shaking water bath as described previously[69].

Human monocyte in vitro experiments

For oxLDL and prosaposin priming experiments, 100,000 cells were added to flat-bottom 96-well plates. After washing with warm PBS, monocytes were incubated either with culture medium only as a negative control, 10 μg/mL oxLDL or 200 ng/mL prosaposin (Abcam, ab203534) for 24 hours (in 10% pooled human serum). Cells were washed once with 200 μl of warm PBS and incubated for 5 days in culture medium with 10% pooled human serum, and medium was refreshed once. Cells were re-stimulated with LPS (10 ng/mL) for 4 hours before applying them to single-cell RNA sequencing in the well-based platform SORT-seq[57]. For cytokine measurements, cells were stimulated with LPS during 24 hours. Subsequently, supernatants were collected and stored at -20 °C until cytokine measurement. In some experiments, cells were pre-incubated (before oxLDL stimulation) for 1 hour with nanobiologics (10 μM mTORi-NB, 0.1 μM S6K1i-NB or corresponding quantities of unloaded NB). After 24 hours, both oxLDL and nanobiologics were washed away and cells were let to rest for 5 days as described above.

Cytokine measurements

Cytokine production was determined in supernatants using commercial ELISA kits for human TNFα and IL-6 following the instructions of the manufacturer.

Single-cell RNA sequencing analysis of human monocytes

For human monocyte single-cell RNA sequencing analysis, the sequencing data was aligned to human hg19 transcriptome. Subsequently *Seurat* (v3.1)[70] was used for downstream analyses. Quality controls were applied to remove low quality cells, which were defined as cells in which fewer than 100 or higher than 7000 unique genes were detected, or cells with higher than 25% mitochondrial counts. Based on a hierarchical clustering of the single-cell RNA profiles we found a subgroup of macrophages with high expression level of chemokine markers (*CXCL9, CXCL10, CXCL11*). By using Wilcoxon rank sum test, differential expression analysis of *PSAP* was performed.

Athero-Express human sample collection

The procedure of obtaining biomaterial of patients elected for endarterectomy within the Athero-Express Biobank Study has been described before [56]. In short, arterial plaque material is obtained during endarterectomy. Each plaque is dissected into segments of 0.5cm. From these, the culprit lesion is reserved for histological assessment (see below). Surrounding segments are either frozen in liquid nitrogen without delay and stored at -80 °C for later use (bulk RNA-seq) or used immediately (single-cell RNA-seq).

Human plaque processing for bulk RNA-seq

In order to assess the global expression profile, plaque segments (n=700) were thawed, cut into pieces, and further homogenized using ceramic beads and tissue homogenizer (Precellys, Bertin instruments, Montigny-le-Bretonneux, France), in the presence of TriPure (Sigma Aldrich). From this homogenized mix RNA was isolated as per TriPure manufacturer's protocol. Then, RNA in the aqueous phase was precipitated with isopropanol, washed with 75% ethanol, and subsequently stored in 75% ethanol for later use or used immediately after an additional washing step with 75% ethanol.

Library preparation for bulk RNA-seq

Library preparation was performed, adapting the CEL-Seq2 protocol for library preparation[71,72], as described before[73]. After removing ethanol, and air-drying the pellet, primer mix containing 5ng primer per reaction was added, initiating primer annealing at 65 °C for 5min. Subsequent reverse-transcription RT reaction; first

strand reaction for 1h at 42 °C, heat inactivated for 10m at 70°C, second strand reaction for 2 hours at 16 °C, and then put on ice until proceeding to sample pooling. This initial RT reaction used the following primer design: an anchored polyT, a unique 6bp barcode, a unique molecular identifier (UMI) of 6bp, the 5' Illumina adapter and a T7 promoter, as described[73]. Each sample now contained its own unique barcode making it possible to pool together cDNA samples at 7 samples per pool. Complementary DNA (cDNA) was cleaned using AMPure XP beads (Beckman Coulter), washed with 80% ethanol, and resuspended in water before proceeding to the *in vitro* transcription (IVT) reaction (AM1334; Thermo-Fisher) incubated at 37 °C for 13 hours. Next, Exo-SAP (Affymetrix, Thermo-Fisher) was used to remove primers, upon which amplified RNA (aRNA) was fragmented, cleaned with RNAClean XP (Beckman-Coulter), washed with 70% ethanol, air-dried, and resuspended in water. After removing the beads by using a magnetic stand, RNA yield and quality in the suspension were checked by Bioanalyzer (Agilent).

cDNA libraries were then built by performing an RT reaction using SuperScript II reverse transcriptase (Invitrogen/Thermo-Fisher) according to the manufacturer's protocol, including randomhexRT primer as random primer. Next, PCR amplification was done with Phusion High-Fidelity PCR Master Mix with HF buffer (NEB, MA, USA) and a unique indexed RNA PCR primer (Illumina) per reaction, for a total of 11-15 cycles, depending on aRNA concentration, with 30 seconds elongation time. PCR products were cleaned twice with AMPure XP beads (Beckman Coulter). Library cDNA yield and quality were checked by Qubit fluorometric quantification (Thermo-Fisher) and Bioanalyzer (Agilent), respectively. Libraries were sequenced on the Illumina Nextseq500 platform; paired end, 2 x 75bp.

Bulk RNA sequencing analysis Athero-Express samples

For bulk RNA-seq analysis of human atherosclerotic plaque samples, fastq files were de-barcoded, and split into forward and reverse reads. These were mapped making use of Burrows-Wheel aligner (BWA)[74] version 0.7.17-r1188, calling 'bwa aln' with settings -B 6 -q 0 -n 0.00 -k 2 -l 200 -t 6 for R1 and -B 0 -q 0 -n 0.04 -k 2 -l 200 -t 6 for R2, 'bwa sampe' with settings -n 100 -N 100, and a cDNA reference (assembly hg19, Ensembl release 84). Read counts and UMI counts were derived from SAM files using custom perl code, and then, using R version 3.6.3 and Rstudio IDE version 1.2.1335 for further analyses, gathered into count matrices. Genes were annotated with Ensembl ID's, and basic quality control was performed. Samples with low gene numbers (<10,000 genes), and read numbers (<18,000 reads) were filtered out. Resulting number of samples: 641, with 60,674 genes (Ensembl ID's), and median of 178,626 reads per sample.

Counts, metadata and clinical data were combined into a SummarizedExperiment object. Counts were pre-filtered, normalized and transformed making use of the variance stabilization transformation function (vst)[75] in DESeq2, resulting in transformed data of n=620 on a log2-scale, normalized for library size. These were used to compare PSAP expression to the expression of a random sample of 1000 genes, and to assess correlations between genes, to construct correlation heatmaps and correlation scatter plots. Correlation estimates and p-values were calculated using Spearman's rank correlation. Heatmaps were drawn using Pheatmap from the Pheatmap package, applying hierarchical clustering based on correlation estimates, applying standard settings: complete linkage and Euclidean distance.

Human plaque processing for single-cell RNA-seq

Plaque segments (n=18) were washed in RPMI and cut up into small pieces (~1mm^3). Nest, tissue was digested using a mix of RPMI 1640, 2.5 mg/mL Collagenase IV (Thermo Fisher Scientific), 0.25 mg/mL DNAse I (Sigma), 2.5 mg/mL Human Albumin Fraction V (MP Biomedicals) and 1 mM Flavopiridol (Selleckchem), incubating at 37 °C for 30 minutes. The resulting cell suspension was filtered using a 70 μm cell strainer and washed with RPMI 1640. Cells were kept in RPMI 1640 containing 1% Fetal Calf Serum until subsequent staining for cell sorting by flow cytometry.

Cell sorting by flow cytometry for single-cell RNA-seq

Cells were washed and then stained with Calcein AM and Hoechst (Thermo Fisher Scientific) in PBS supplemented with 5% Fetal Bovine Serum (FBS) and 0.2% ethylenediaminetetraacetic acid (EDTA) for 30 minutes at 37 °C. Subsequently, cells were washed, filtered (70 μm FlowMi cell strainer; SP Scienceware), upon which Calcein AM and Hoechst double-positive viable cells were sorted using a MoFlo Astrios EQ cell sorter (Beckman Coulter).

Single cell RNA-sequencing

Viable cells were single-cell sorted into these 384 wells plates containing 50 nL mineral oil, CELseq2-primers, spike-ins and dinucleotide triphosphates (dNTPs). Afterwards, plates were immediately sealed and frozen at -80 °C until further processing. First, cDNA was constructed using the SORT-seq protocol[57]. In short, cells were lysed for 5 minutes at 65 °C upon which reverse transcription and second strand mixes were making use of a Nanodrop II liquid handling platform (GC biotech) Then, cells were pooled into one library. The aqueous phase was separated from the oil phase, followed by *in vitro* transcription (IVT). The CEL-Seq2 protocol[71,72] was used to construct a library, with the following primers design: a 24 bp polyT stretch, a 64bp random UMI, a cell-specific 8bp barcode, the 5′ Illumina TruSeq small RNA kit

adapter and a T7 promoter. For sequencing, TruSeq small RNA primers (Illumina) were added to the libraries and sequenced paired end at 75 bp read length using an Illumina NextSeq 500.

Single-cell RNA-sequencing analysis

Athero-Express samples Prior to processing, reads were filtered for mitochondrial and ribosomal genes, MALAT1, KCNQ1OT1, UGDH-AS1, and EEF1A. Then, remaining single-cell sequencing data was processed as described previously[57] in an R 3.5 environment using Seurat (version 2.3.4)[58]. Cells expressing between 500 and 10.000 genes and genes expressed in at least 3 cells were used for further analysis. Data was log-normalized and scaled with the exclusion of UMIs. Canonical correlation analysis (CCA) reduction was performed, resolution set to 1.2 for 15 dimensions, in order to identify clusters and to perform t-distributed stochastic neighbor embedding (t-SNE). Cell clusters were annotated by evaluating differential gene expression of individual cell clusters (Wilcoxon rank sum test) and analyzing against BLUEPRINT[59] reference data using SingleR[60].

Statistical analysis

Data are shown as mean ± SD, unless otherwise stated. For plaque volume analysis, either an unpaired t-test or a one-way ANOVA with Dunnett's correction were applied depending on the number of groups. For in vitro human monocyte experiments, normality checks were performed using gg-plots and a normality assay. Non-parametric parameters were analyzed pairwise using a Wilcoxon signed-rank test. Correlations between genes in human bulk RNA sequencing were calculated by Spearman coefficients. Significance of differences in all other experiments was calculated using non-parametric Mann-Whitney U tests. Two-sided testing was used and a p-value below 0.05 was considered statistically significant. For mouse transcriptome analyses, false discovery rate control was applied and adjusted p-values were reported. All data were analyzed using Graphpad Prism version 8.4.3. *$p<0.05$, **$p<0.01$, ***$p<0.001$, ****$p<0.0001$.

ACKNOWLEDGMENTS

9

Funding

Author contributions

R.D. and W.J.M.M. designed the study. M.M.T.v.L., T.J.B., Y.C.T., M.L., S.B., S.A.N., N.R., C.P.-M., E.K., E.A.F., F.K.S., M.N., E.L., L.A.B.J., Z.A.F., M.G.N., N.P.R., W.J.M.M., and R.D. designed, performed and oversaw the *in vivo, in vitro* and *ex vivo* experiments. F.F., B.L.S.-G. and M.L. developed and produced the nanobiologics. A.J.P.T., E.D.K. and R.v.d.M. designed and formulated the siRNA lipid nanoparticles. Flow cytometry, histology, immunostaining and laser capture microdissection were performed and analyzed by M.M.T.v.L., T.J.B., J.M., M.L., and R.D. FMT/CT was performed and analyzed by R.D., Y.-X.Y., G.W. and M.N. Metabolic studies were performed and analyzed by T.J.B. RNA sequencing and transcriptome analysis of mouse atherosclerotic tissue was performed and analyzed by X.Z., B.Z., M.L., M.M.T.v.L. and R.D. RNA sequencing and transcriptome analysis of human atherosclerotic tissue was performed and analyzed by G.P., A.B., and R.D. The immune cell priming experiments with human monocytes were performed and analyzed by B.Z., Y.L., S.B. and N.P.R. The manuscript was written by M.M.T.v.L., W.J.M.M. and R.D. All authors contributed to the writing of the manuscript and approved the final draft. Z.A.F., W.J.M.M., and R.D. provided funding.

Competing interest

Z.A.F., W.J.M.M., M.G.N., L.A.B.J. are founders of Trained Therapeutix Discovery.

Data and materials availability

All data associated with this study are in the paper or supplementary materials. Mouse RNA sequencing data are available at the Gene Expression Omnibus (GEO) database (GEO series number GSE104777). Human atherosclerotic plaque R scripts are available through GitHub [https://github.com/AtheroExpress/MicroanatomyHumanPlaque_scRNAseq].

SUPPLEMENTAL TABLES

Gene	Chemokine	Log FC	Adjusted P-value
Ccl2	CCL2	0.31296	0.65576952
Ccl3	CCL3	-0.39280	0.5613907
Ccl5	CCL5	0.18974	0.91805817
Ccl19	CCL19	-0.43587	0.5127425
Cxcl1	CXCL1	0.83790	0.63716585
Pf4	CXCL4	-1.24206	0.17567479
Cxcl5	CXCL5	1.17180	0.48393745
Ccl17	CCL17	1.08535	0.36512255
Mif	MIF	-0.53858	0.17672978
Cxcl12	CXCL12	-0.49165	0.0983902
Cx3cl1	CX3CL1	0.79874	0.0523904

Table S1. Expression of genes coding for chemokines after mTORi-NB treatment. Gene expression in plaque monocytes and macrophages as compared to PBS control.

Gene	Chemokine	Log FC	Adjusted P-value
Ccl2	CCL2	-0.00716	0.99102237
Ccl3	CCL3	0.24487	0.64175807
Ccl5	CCL5	0.06486	0.95931883
Ccl19	CCL19	0.19736	0.7281466
Cxcl1	CXCL1	1.36319	0.24059588
Pf4	CXCL4	-0.53844	0.45338915
Cxcl5	CXCL5	0.52422	0.73728945
Ccl17	CCL17	0.77033	0.43047021
Mif	MIF	-0.31895	0.33069264
Cxcl12	CXCL12	0.27087	0.28619421
Cx3cl1	CX3CL1	1.04888	0.00247937

Table S2. Expression of genes coding for chemokines after S6K1i-NB treatment. Gene expression in plaque monocytes and macrophages as compared to PBS control.

Gene	Log FC	Adjusted P-value
Akt1	-0.06322	0.9104776
Ambra1	0.47820123	0.17869625
App	-0.239403	0.23855464
Arsa	0.21776034	0.79553701
Atg10	0.08458822	0.9259492
Atg12	-0.4014704	0.38758432
Atg16l1	0.27097739	0.67061
Atg16l2	0.43691291	0.58220107
Atg3	-0.2365799	0.39150025
Atg4a	0.04417891	0.97013377
Atg4b	-0.1048479	0.91974653
Atg4c	0.13199719	0.82116451
Atg4d	0.51338288	0.71720056
Atg5	-0.1456187	0.80253625
Atg7	0.1333619	0.75482858
Atg9a	0.58674968	0.48431597
Atg9b	0.44118666	0.81182536
Bad	0.41721449	0.67110694
Bak1	-0.0731939	0.91974653
Bax	-0.5025847	0.08191031
Bcl2	0.00557685	0.99301165
Becn1	0.17303877	0.8389349
Bid	-0.3569908	0.47237531
Bnip3	0.11370475	0.91221636
Cln3	-0.0844936	0.84365585
Cxcr4	-0.5255795	0.40118318
Dram1	0.04323607	0.94370751
Dram2	-0.195949	0.67061
Eif2ak3	0.02590746	0.96993217
Eif4g1	0.42907678	0.21925935
Eva1a	-0.4900791	0.7507438
Gaa	0.10936266	0.85832283
Gabarap	-0.3068282	0.30774929
Gabarapl1	0.13655259	0.76131999
Gabarapl2	-0.2891248	0.44397101
Hgs	-0.0407813	0.96161318
Htt	0.10947356	0.79690999
Map1lc3a	0.27861007	0.75731551
Map1lc3b	-0.0302392	0.94218139

Gene	Log FC	Adjusted P-value
Pik3c3	0.0621041	0.93584142
Pik3r4	-0.1843173	0.70671046
Pten	-0.097594	0.76453618
Rab24	0.00083353	0.99887287
Rgs19	-0.0735851	0.8801925
Snca	0.56471989	0.8314463
Sqstm1	-0.2376393	0.56678557
Ulk1	0.1587401	0.78201071
Uvrag	0.16747522	0.73636682
Vps11	-0.2863072	0.45699772
Vps18	0.03380649	0.95995687
Wipi1	-0.1570408	0.80540665
Wipi2	0.28947189	0.65660035

Table S3. Expression of autophagy-related genes after mTORi-NB treatment. Gene expression in monocytes and macrophages as compared to PBS control.

9

Gene	Log FC	Adjusted P-value
Akt1	-0.0963084	0.77965886
Ambra1	0.64609418	0.02107062
App	-0.3048642	0.06212166
Arsa	0.53462818	0.26375584
Atg10	-0.0908332	0.8721451
Atg12	-0.5251236	0.12628148
Atg16l1	0.73261294	0.05882449
Atg16l2	0.25736148	0.691515
Atg3	-0.4113048	0.04364753
Atg4a	-0.518344	0.3527245
Atg4b	0.26418674	0.62259324
Atg4c	0.11796574	0.77911201
Atg4d	0.55149709	0.57776291
Atg5	-0.0468501	0.91691084
Atg7	0.56047154	0.02530181
Atg9a	1.00205938	0.07792097
Atg9b	-0.0311676	0.98354763
Bad	0.53327754	0.42217156
Bak1	0.29589511	0.40124234
Bax	-0.6978604	0.00407231
Bcl2	0.46300037	0.07631071
Becn1	0.19421811	0.73879352
Bid	-0.2469348	0.5277853
Bnip3	0.06968356	0.91630588
Cln3	0.24233459	0.32107786
Cxcr4	-0.433262	0.38963682
Dram1	-0.3628319	0.18234813
Dram2	-0.2952424	0.35684941
Eif2ak3	-0.109087	0.77131365
Eif4g1	0.43493143	0.12162772
Eva1a	-1.8358585	0.07683732
Gaa	0.26790526	0.46088664
Gabarap	-0.1397243	0.61224856
Gabarapl1	0.0356016	0.92685945
Gabarapl2	-0.8377508	0.00398818
Hgs	0.40132319	0.29166243
Htt	0.20689677	0.44036163
Map1lc3a	0.12440222	0.86633139
Map1lc3b	-0.2246937	0.2339822

Gene	Log FC	Adjusted P-value
Pik3c3	0.13499383	0.74692382
Pik3r4	-0.2055543	0.55438368
Pten	-0.1190931	0.61065606
Rab24	-0.4228867	0.14585505
Rgs19	0.19202575	0.48512655
Snca	-0.4988481	0.80875403
Sqstm1	-0.3630585	0.22598883
Ulk1	0.4695546	0.15327301
Uvrag	0.06612864	0.87435194
Vps11	-0.0552954	0.87989096
Vps18	0.05708651	0.88811304
Wipi1	-0.2248268	0.58860276
Wipi2	0.17827191	0.73373098

Table S4. Expression of autophagy-related genes after S6K1i-NB treatment. Gene expression in plaque plaque monocytes and macrophages as compared to PBS control.

Gene	Log FC	Adjusted P-value
Psap	-1.0278619	0.01572881
Ctsb	-0.988728	0.01509807
Cox7c	-0.745240103	0.04504972
Rsrp1	-1.184914126	0.01549977
Synpo	0.836086035	0.03921505
Flna	0.68071212	0.0305352
Hspg2	0.98632714	0.03921505

Table S5. Hub genes of the mTORi-NB-related *turquoise* module.

Gene	Log FC	Adjusted P-value
Hnrnph	-0.674369135	0.009427671
Psap	-1.219198958	0.001464033
Rps27a	-1.170438898	0.000312172
Cox7c	-1.048638001	0.001262728
Lyz1	-1.14486756	0.000957917
Rn45s	2.281255556	0.00294076
Arhgdia	0.928242972	0.000311025

Table S6. Hub genes of the S6K1i-NB-related *turquoise* module.

9

Gene	Estimate	Statistic	P-value
AKT1	0.45165527508346365	21780926.937696468	1.71e-32
AKT1S1	0.34156205070403	26153965.224713564	2.09e-18
AKT2	0.08315045831289128	36418391.520748235	0.0385
CAB39	0.5512671378955364	17824221.224209685	1.41e-50
CAB39L	0.1418716983315031	34085911.640083745	3.95e-4
EEF2K	0.08099246289773902	36504109.75297245	0.0438
EIF4B	0.680881553419964	12675777.213848323	1.21e-85
EIF4E	-0.338832264388465	53180064.305195026	4.03e-18
EIF4EBP1	0.6051334881203897	15684583.537667735	3.38e-63
EIF4G1	0.5043801091984009	19686631.675105203	2.55e-41
LAMTOR1	0.7775665915236178	8835328.577774325	1.25e-126
LAMTOR2	0.7117106866601788	11451206.121713107	7.42e-97
LAMTOR3	0.20423869897231745	31608617.663219813	2.91e-7
LAMTOR4	0.6263585657750161	14841497.346380455	7.29e-69
LAMTOR5	0.6972815335140743	12024349.832534747	1.98e-91
MLST8	0.21150426467196057	31320020.456984177	1.06e-7
MTOR	0.38067708066467343	24600268.123189956	8.18e-23
PPM1A	0.631498249138613	14637342.801367851	2.65e-70
PRKAA1	0.30219385332589715	27717718.447455775	1.47e-14
PRKAA2	-0.1073000560849059	43983320.20676145	0.00749
PRKAB1	-0.24542888810671235	49469967.31313098	5.87e-10
PRKAB2	0.37397620432482104	24866435.173486788	5.14e-22
PRKAG1	0.3066746305219916	27539736.46587095	5.73e-15
PRKAG2	0.2800286319529117	28598148.303613048	1.24e-12
PRKAG3	-0.025663298778574425	40740607.79334247	0.524
RHEB	0.6176288482847785	15188252.462645208	1.76e-66
RPS6	0.7916053124362363	8277693.315498397	2.48e-134
RPS6KB1	0.19834135925734458	31842867.250426386	6.42e-7
RPTOR	0.12087189434866864	34920049.68404084	0.00257
RRAGA	0.6258121557234727	14863201.425712124	1.03e-68
RRAGB	0.09268856732085305	36039526.09907791	0.0210
RRAGC	0.36072147214944505	25392929.4388133	1.73e-20
RRAGD	0.59491515714112575	16090468.212711202	1.28e-60
SLC38A9	0.04559822970010717	37910012.23048921	0.257
STK11	0.24463154847624402	30004163.99771896	6.70e-10
STRADA	0.689009565168165	12352922.589755328	1.84e-88
STRADB	0.29917553704996575	27837609.68246479	2.75e-14
TSC1	0.139868851242274	34165467.189969845	4.78e-4
TSC2	0.31993049962144865	27013197.04052152	3.20e-16
YWHAB	0.8807236194960035	4737804.54356676	9.62e-203

Table S7. Correlation between *PSAP* expression and genes involved in mTOR signaling.

Gene	Estimate	Statistic	P-value
APOC1	0.9243210590782618	3006060.6185087753	9.67e-261
APOE	0.9096722167363649	3587930.654405001	5.16e-238
CCL2	0.819791720688361	7158094.510441854	9.40e-152
CCL5	0.0997016473963565	35760957.93239043	0.0130
CTSB	0.9384039558518568	2446670.6366985515	2.12e-287
CTSD	0.9664343657524052	1333268.278044592	0
CXCL2	0.3317131964009651	26545173.831722096	2.17-17
CXCL3	0.48329063154314544	20524331.667629465	1.32e-37
CXCL8	0.3337046358241323	26466071.408363402	1.36e-17
IL1A	0.09889415971657174	35793032.33624132	0.0138
IL1B	0.370062481056971	25021893.075565413	1.48e-21
IL6	0.1324453697499877	34460337.0057257	9.47e-4
MMP9	0.7988011370403015	7991866.311360664	1.63e-138
NFKB1	0.5498090778999125	17882137.160649657	2.88e-50
NFKB2	0.38949215580494645	24250122.496075887	6.81e-24
NLRP3	0.02850960343379891	38588793.484797284	0.479
REL	-0.3503838349268979	53638906.89541335	2.39e-19
RELA	0.3782530901288295	24696552.008782033	1.60e-22
RELB	0.5603963310277618	17461598.44409014	1.49e-52
TNF	0.1541101644040152	33599784.714370295	1.17e-4

Table S8. Correlation between *PSAP* expression and genes involved in macrophage inflammation.

9

SUPPLEMENTAL FIGURES
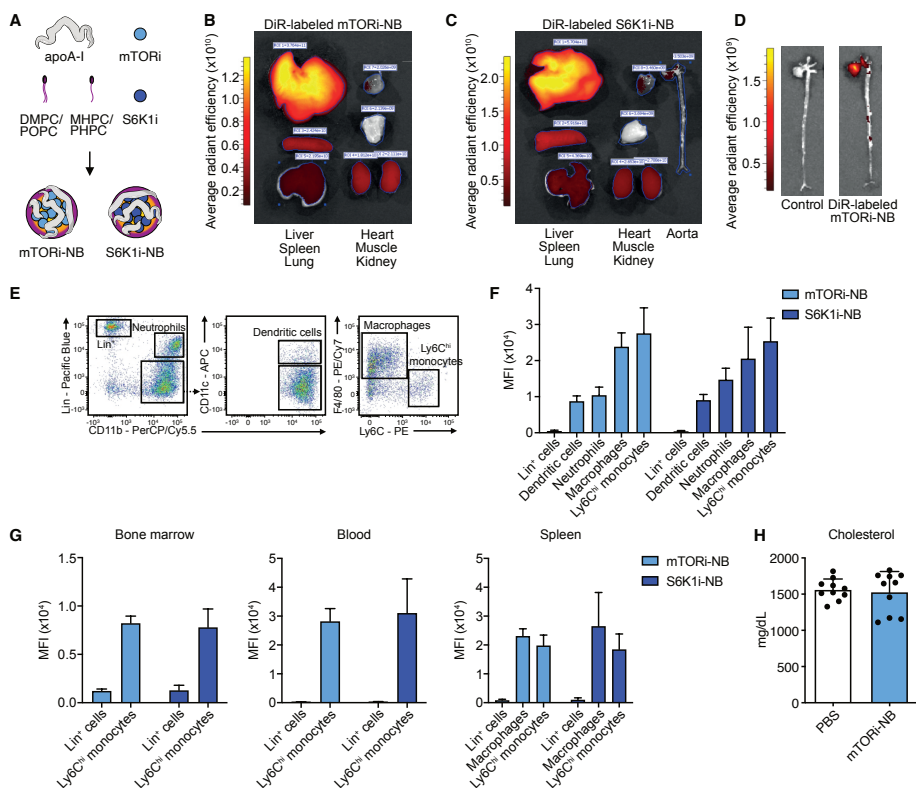
Figure S1. Characteristics of mTORi-NB and S6K1i-NB. Related to Figure 1. (**A**) Schematic overview of the different components of mTORi-NB and S6K1i-NB. mTORi-NB was constructed by combining human apoA-I, the phospholipids DMPC and MHPC and the mTOR inhibitor rapamycin. S6K1i-NB consisted of apoA-I, the phospholipids POPC and PHPC, and the S6K1 inhibitor PF-4708671. (**B,C**) IVIS imaging of organs of *Apoe*^{-/-} mice, injected with DiR-labeled mTORi-NB (**B**) or DiR-labeled S6K1i-NB (**C**). Organs were harvested 24 hours after injection. (**D**) IVIS imaging of the aorta of DiR-labeled mTORi-NB injected *Apoe*^{-/-} mice. (**E-G**) *Apoe*^{-/-} mice were injected with DiO-labeled mTORi-NB or DiO-labeled S6K1i-NB and sacrificed 24 hours later. (**E**) Flow cytometry gating strategy of CD45^{+} cells in the whole aorta and (**F**) quantification of DiO signal in each cell type. (n=2-4 per group). (**G**) Quantification of DiO signal in leukocyte populations in the spleen, bone marrow and blood. (n=4). (**H**) *Apoe*^{-/-} mice were kept on a Western diet for 12 weeks, followed by 1 week of treatment, while continuing the diet. Treatment consisted of 4 intravenous injections of control (PBS) or mTORi-NB. Graph shows blood cholesterol levels of *Apoe*^{-/-} mice after mTORi-NB treatment as compared to control.

Data are presented as mean ± SD. *p<0.05, **p<0.01, ***p<0.001, ****p<0.0001.
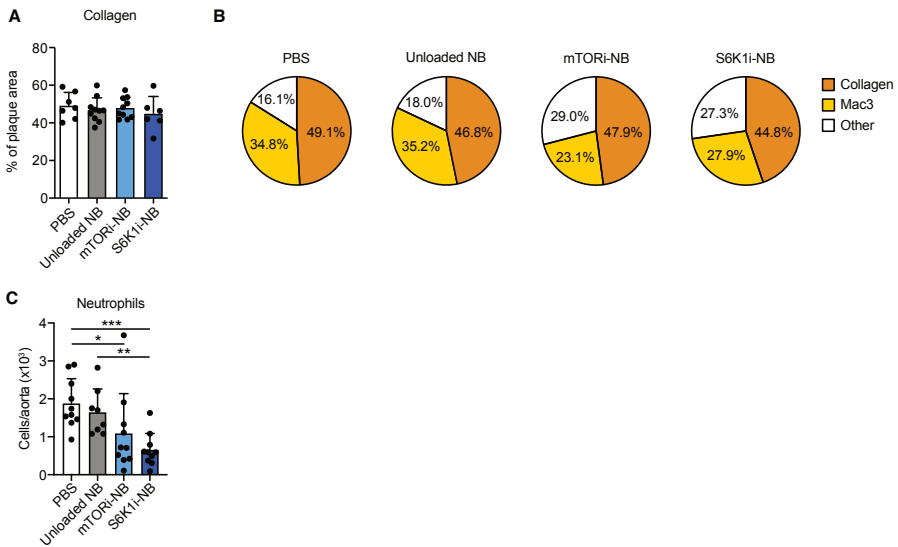
Figure S2. Myeloid cell-specific mTOR inhibition reduces atherosclerotic plaque inflammation. Related to Figure 1. *Apoe*^{-/-} mice were kept on a Western diet for 12 weeks, followed by 1 week of treatment, while continuing the diet. Treatment consisted of 4 intravenous injections of control (PBS), unloaded nanobiologics, mTORi-NB or S6K1i-NB. (**A**) Collagen content expressed as percentage of plaque area, assessed by Sirius Red staining (n=6-10 per group). (**B**) Relative contributions of collagen and Mac3+ areas to the aortic plaque. (**C**) Flow cytometry analysis of neutrophils (CD11b+Lin+) in the aorta (n=8-10 per group). Bar graphs are presented as mean ± SD.*p<0.05, **p<0.01, ***p<0.001, ****p<0.0001.
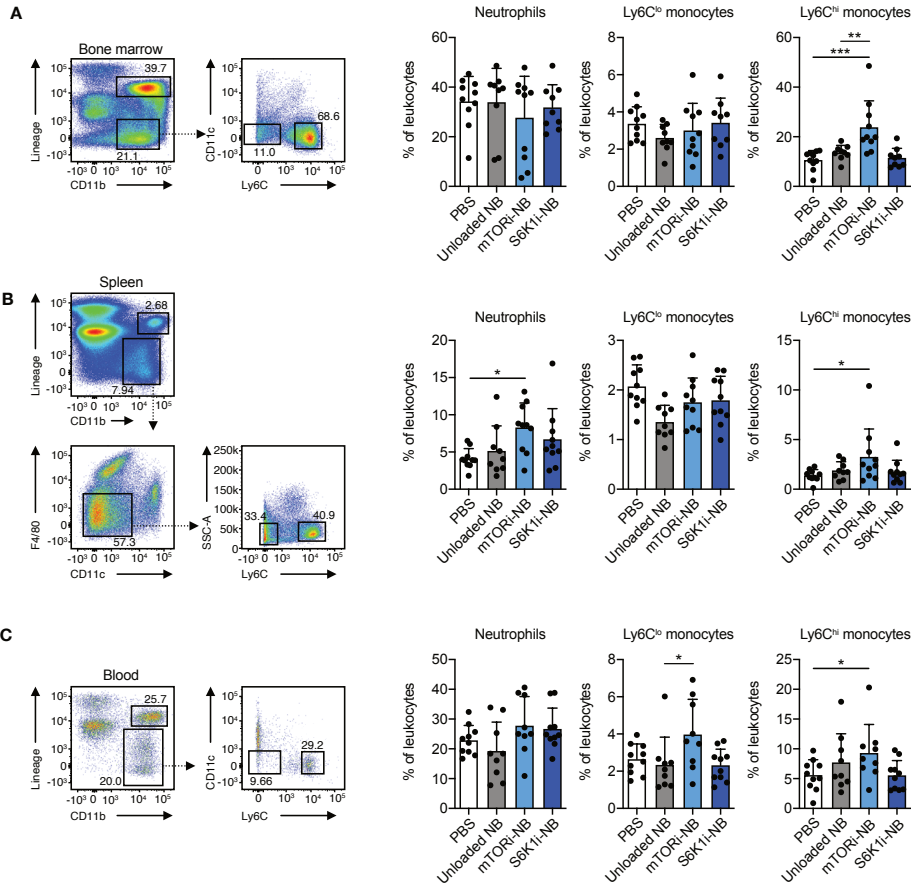
Figure S3. Systemic effects of mTORi-NB and S6K1i-NB treatment. Related to Figure 1. *Apoe⁻/⁻* mice were kept on a Western diet for 12 weeks, followed by 1 week of treatment, while continuing the diet. Treatment consisted of 4 intravenous injections of control (PBS), unloaded nanobiologics, mTORi-NB or S6K1i-NB (n=9-10 per group for all panels). (**A**) Gating strategy and quantification of neutrophils (CD11b⁺Lin⁺), Ly6C^lo (CD11b⁺Lin⁻CD11c⁻Ly6C^lo) and Ly6C^hi (CD11b⁺Lin⁻CD11c⁻Ly6C^hi) monocytes in the bone marrow. (**B**) Gating strategy and quantification of neutrophils (CD11b⁺Lin⁺), Ly6C^lo (CD11b⁺Lin⁻CD11c⁻F4/80⁻Ly6C^lo) and Ly6C^hi (CD11b⁺Lin⁻CD11c⁻F4/80⁻Ly6C^hi) monocytes in the spleen. (**C**) Gating strategy and quantification of neutrophils (CD11b⁺Lin⁺), Ly6C^lo (CD11b⁺Lin⁻CD11c⁻Ly6C^lo) and Ly6C^hi (CD11b⁺Lin⁻CD11c⁻Ly6C^hi) monocytes in peripheral blood. Bar graphs are presented as mean ± SD, *p<0.05, **p<0.01, ***p<0.001, ****p<0.0001.
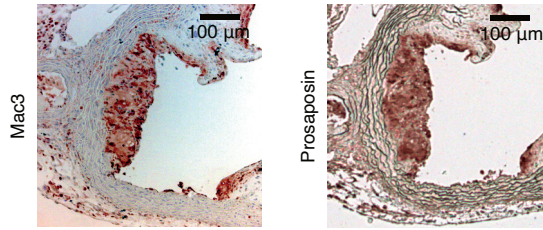
Figure S4. Prosaposin colocalizes with macrophages in murine plaques. Related to Figure 2. Representative histologic images of murine atherosclerotic plaques. Staining for macrophages (Mac3) correlates with prosaposin staining.
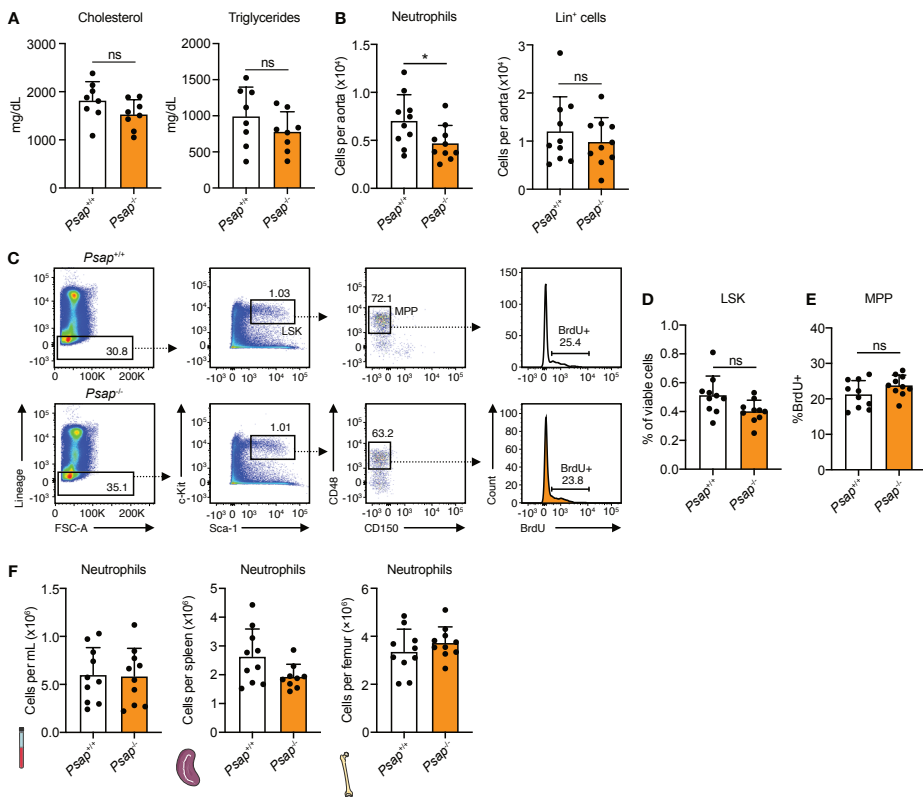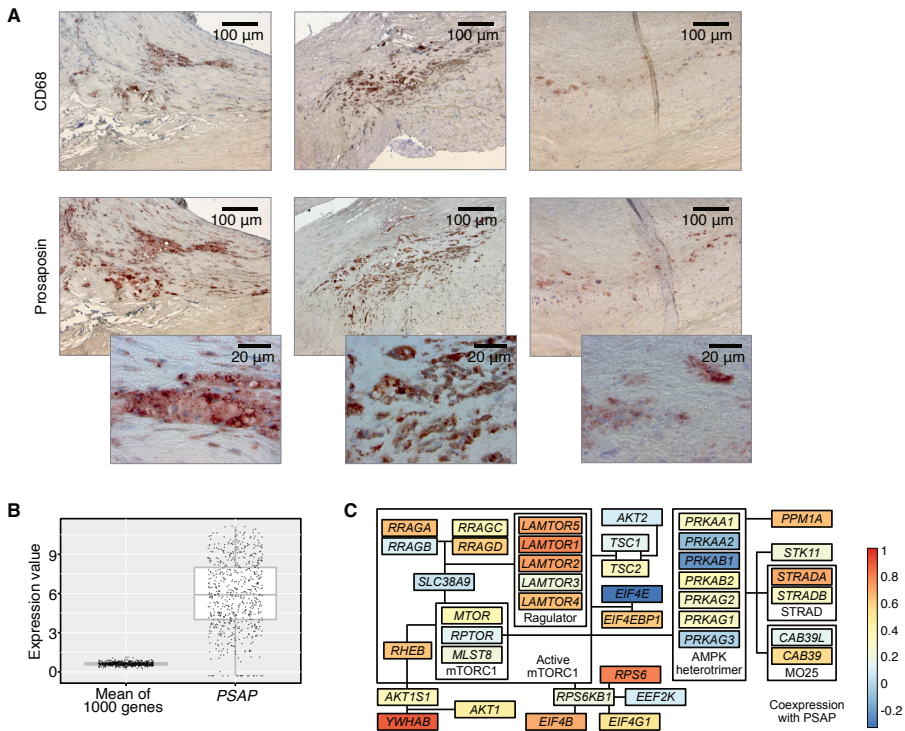

Figure S5. *Psap* **mediates atherosclerotic plaque inflammation in** *Ldlr*^{-/-} **mice.** Related to Figure 4. *Ldlr*^{-/-} mice were lethally irradiated and transplanted with *Psap*^{+/+} or *Psap*^{-/-} bone marrow cells. Mice were left to reconstitute for 6 weeks after which they were put on a Western diet for 11 weeks (n=10 for all panels). (**A**) Blood cholesterol and triglyceride levels of *Ldlr*^{-/-} mice transplanted with *Psap*^{+/+} or *Psap*^{-/-} bone marrow after 11 weeks of Western diet. (**B**) Flow cytometry analysis of neutrophils (CD11b^{+}Lin^{+}) and lineage positive (Lin^{+}) cells in the aorta of *Psap*^{+/+} and *Psap*^{-/-} transplanted mice. (**E**) Representative flow cytometry plots and (**F**) quantification of lineage negative, Sca1 positive, c-kit negative (LSK) cells in the bone marrow. (**G**) *Ldlr*^{-/-} mice were injected with 1 mg of BrdU, 24 hours before sacrifice. Graph shows quantification of BrdU positive multipotent progenitors (MPPs). (**H**) Neutrophils in the blood, spleen and bone marrow as assessed by flow cytometry. Data are presented as mean ± SD. *p<0.05, **p<0.01, ***p<0.001.
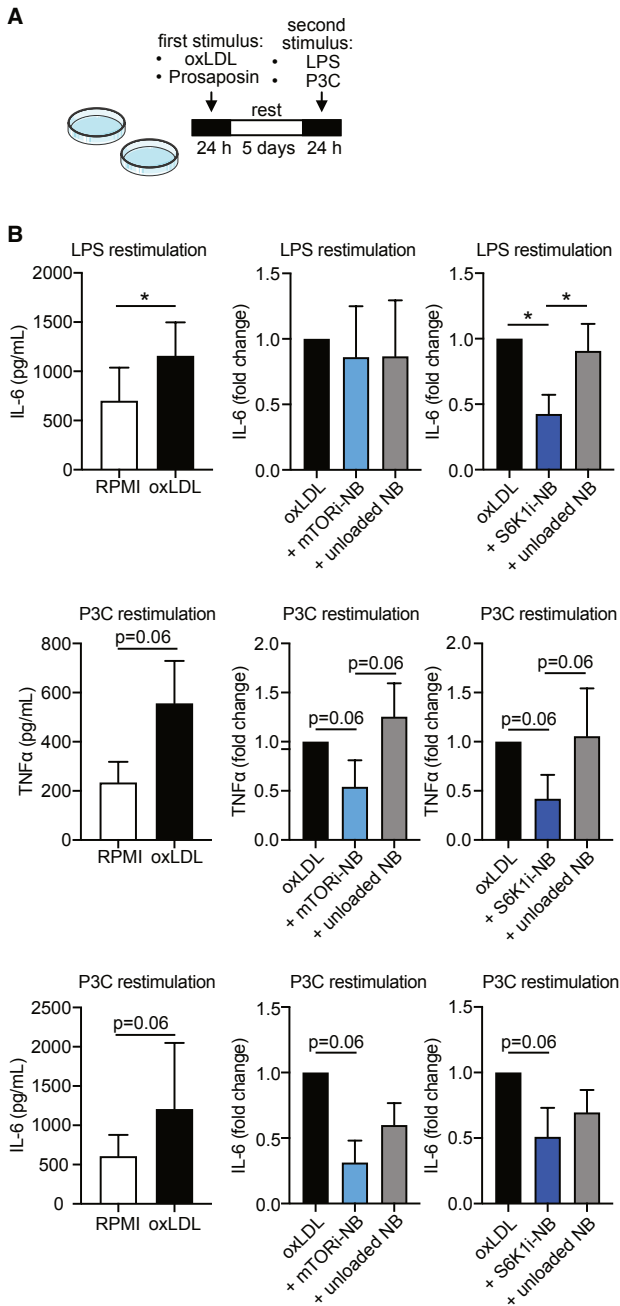
Figure S6. Nanobiologics inhibit oxLDL priming in human monocytes. Related to Figure 5. Human primary monocytes were primed with oxidized LDL (oxLDL), in combination with mTORi-NB, S6K1i-NB, unloaded NB or RPMI for 24 hours. After a 5-day rest, cells were restimulated with LPS or Pam3Cys. TNFα or IL-6 production were measured by ELISA. This *in vitro* assay is schematically shown in A. (**B**) OxLDL amplifies the cytokine response, but this can be mitigated by both nanobiologics (n=5-6).

Figure S7. *PSAP* **mediates atherosclerotic plaque inflammation in humans.** Related to Figure 5. (**A**) Additional images of CD68 (top) and prosaposin (middle and bottom) staining on human carotid endarterectomy samples. Prosaposin is abundantly expressed in the plaque and colocalizes with CD68-positive areas.

(**B,C**) Transcriptomic analyses were performed on human atherosclerotic plaques (n=620). (**B**) Gene expression level of *PSAP* as compared to the average expression level of 1000 random genes was assessed showing that *PSAP* expression in the plaque is markedly higher than what can be assumed from a randomly selected gene. (**C**) Schematic representation of the genes encoding for mTOR signaling proteins. Color depicts their co-expression with *PSAP*.
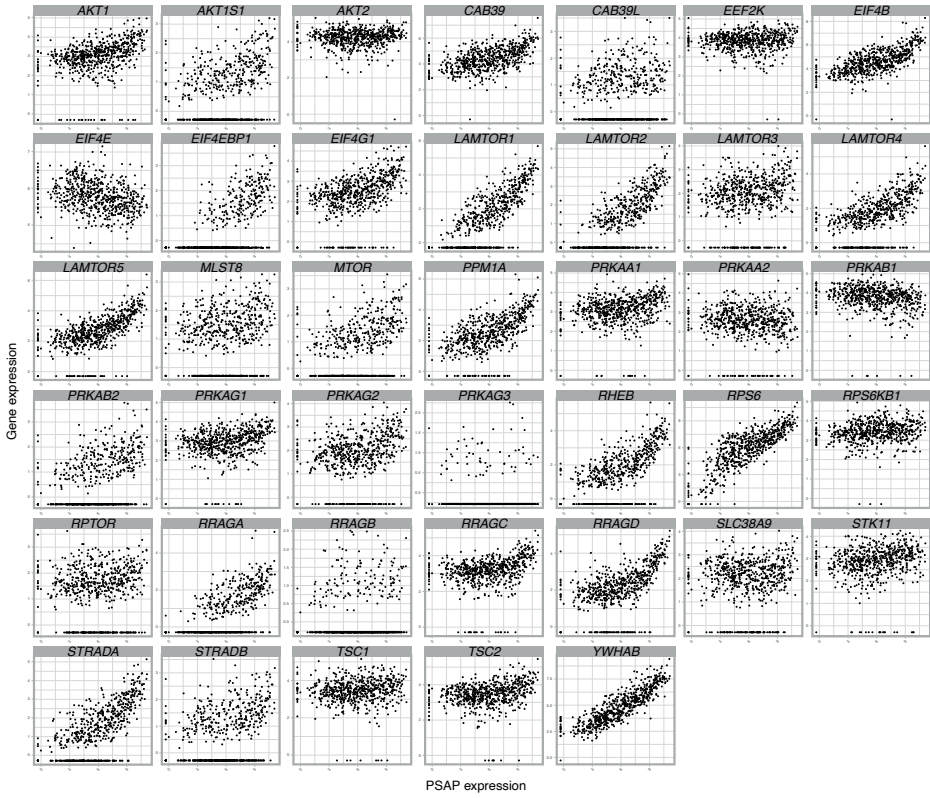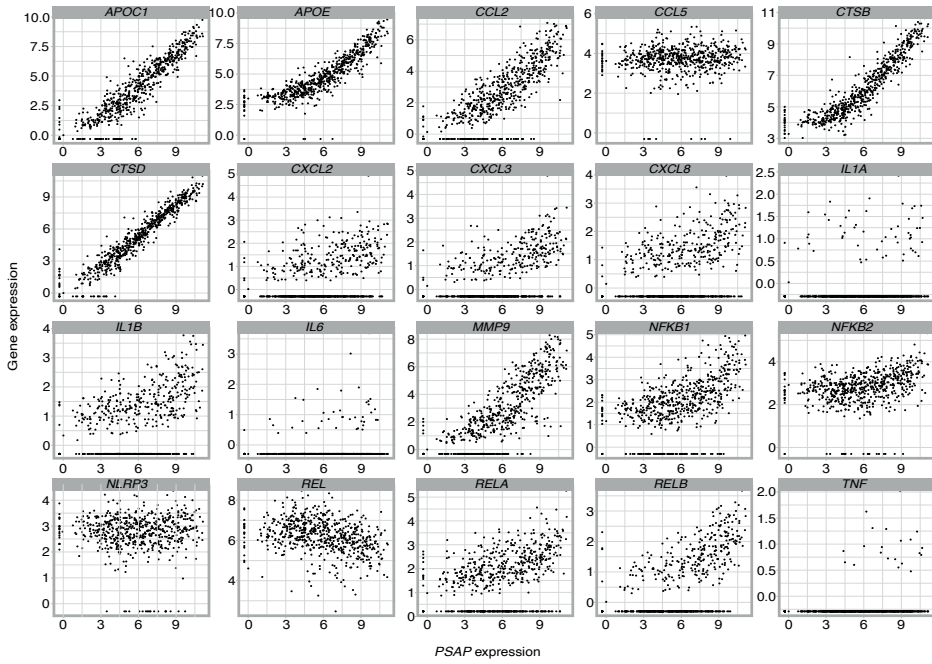
Figure S8. Correlation between *PSAP* expression and genes involved in mTOR signaling or macrophage inflammation. Related to Figure 5. Transcriptomic analyses were performed on human atherosclerotic plaques (n=620). (**A**) Expression of PSAP is plotted against 40 genes involved in the mTOR signaling pathway. Each dot represents one saple. (**B**) Expression of PSAP is plotted against 20 genes that define macrophage subsets in human atherosclerotic plaque.

Fig. S9. Correlation between *PSAP* expression and genes involved in macrophage inflammation. Related to Fig. 5. Transcriptomic analyses were performed on human atherosclerotic plaques ($n = 620$). Expression of PSAP is plotted against 20 genes that define macrophage subsets in human atherosclerotic plaque. Each dot represents one sample.